Comparison of Creep Compliance Master Curve Models for Hot Mix Asphalt

Myunggoo Jeong

Thesis submitted to the faculty of the Virginia
Polytechnic Institute and State University in partial fulfillment of the requirements for the degree of

Master of Science
In
Civil and Environmental Engineering

Dr. Gerardo Flintsch, Co-Chair
Dr. Amara Loulizi, Co-Chair
Dr. Antonio Trani

July, 2005

Blacksburg, Virginia

Keyword: Viscoelasticity, Creep Compliance, Interconversion, Hot Mix Asphalt

Comparison of Creep Compliance Master Curve Models for Hot Mix Asphalt

Myunggoo Jeong

Abstract

The creep compliance of Hot Mix Asphalt (HMA) is an important property in characterizing the material's viscoelastic behavior. It is used to predict HMA thermal cracking at low temperature and permanent deformation at high temperatures. There are several experimental methods to measure the creep compliance. Two of these methods were used in this thesis: the uniaxial compressive and indirect tension (IDT) creep compliance. The tests were conducted at five temperatures (-15, 5, 20, 30, and 40°C) with a static loading for 1000-sec to characterize two typical HMA mixes used in Virginia, a base and a surface mix. Creep compliance master curves (CCMC) were developed by shifting the curves to a reference temperature using time-temperature superposition. Three mathematical functions, the Prony series, power and sigmoidal, were fitted to the experimental data using regression analysis. Uniaxial CCMC were also predicted based on dynamic modulus measurements using method for interconversion of vicoelastic properties recommended in the literature. Finally, the susceptibility of the mixes to thermal cracking was evaluated based on the creep compliance measurements at low temperature.

The regression analysis showed that the three mathematical models considered are appropriate to model CCMC over a wide range of reduced times. The sigmoidal model provided the best fit over the entire range of reduced times investigated. This model also produced the best results when used in the interconversion procedures. However, there were noticeable differences between the CCMC predicted using interconversion and the experimental measurements, probably due to nonlinearity in the material behavior. The m-values for the base mix were higher than those for the surface mix using the creep results measured with both configurations.

Acknowledgements

I would like to express my utmost appreciation to my advisor, Dr. Flintsch for his time, patience and advice. He has provided me with several opportunities to do research. I could not have done this thesis without his support. I also would like to thank Dr. Loulizi, who has always advised me as a co-chair, mentor and friend. He took the time to listen to me and advised me whenever I faced unexpected problems. I would like to extend my gratitude also to my thesis committee, Dr. Trani for his valuable comments and suggestions.

I would also like to thank my colleagues at the Virginia Tech Transportation Institute: I express my gratitude to Billy and Samer in the asphalt lab, who helped me prepare lab-tests and answered a number of questions I asked. I am also grateful to Aris, Carlos, Chen Chen, Edgar, Hao, Jae, Sangjun and Zheng.

I owe many thanks to my fiancé, Kyung-A, for her unending love and understanding. She will hold a special place in my heart until the end of my life.

Finally, I am grateful to my brothers, Wan Goo and Bong Goo for their support and care throughout my life, and to my beloved mother, Choon Ae Kim who is the meaning of my life and the reason I breathe. I appreciate her sacrifice, endurance and endless love.

TABLE OF CONTENTS

Chapter 1 Introduction 1
1.1. Background 1
1.2. Problem Statement 2
1.3. Objectives 2
1.4. Significance 3
1.5. Research Scope 3
Chapter 2 Literature Review 4
2.1. Introduction 4
2.2. The Creep Compliance 4
2.2.1. Creep Compliance Test Configurations 6
2.2.2. Creep Compliance Models 8
2.3. The Relaxation Modulus 10
2.4. Time-Temperature Superposition and Master Curve 12
2.5. Dynamic (Complex) Modulus 14
2.6. Sigmoidal Functions for Modeling Mater Curves 17
2.7. Interconversion among Viscoelastic Material Properties 18
2.7.1. Interconversion between the Relaxation Modulus and Creep Compliance… 18
2.7.2. Interconversion between the Relaxation Modulus / Creep Compliance and Dynamic Modulus 20
2.8. Thermal Cracking Models 21
2.8.1. Empirical-based Models for Thermal Cracking on Flexible Pavement 22
2.8.2. Mechanistic-based Models 23
2.8.3. M-E Design Guide Model (2002) 24
Chapter 3 Experimental Program 27
3.1. Introduction 27
3.2. Sample Preparation and Conditioning 27
3.3. Test Methods 31
3.3.1. Uniaxial Creep Test 31
3.3.2. Indirect Tensile Creep Test 32
3.4. Test Results 33
Chapter 4 Creep Compliance Master Curves 37
4.1. Introduction 37

4.2. Fitting Creep Compliance Master Curve Models 37
4.2.1. CCMC Construction 37
4.2.2. CCMC Mathematical Model Fitting 40
4.3. Effect of the Thermal Cracking Model using the *m*-value 47
4.4. Summary 50
Chapter 5 Interconversion between the Dynamic Modulus and Creep Compliance 51
5.1. Introduction 51
5.2. Conversion from the Dynamic Modulus to Creep Compliance 51
5.2.1. Prediction of the Relaxation Modulus from the Dynamic Modulus 51
5.2.2. Prediction of the Creep Compliance from the Relaxation Modulus 54
5.2.3. Comparison of Computed versus Measured Creep Compliances 55
5.3. Comparison from the Creep Compliance to the Dynamic Modulus 57
5.4. Summary 59
Chapter 6 Findings, Conclusions, and Recommendations 60
6.1. Findings 60
6.2. Conclusions 61
6.3. Recommendations 61
References 63
Appendix A: Fitting model SAS Input and Output 66

List of Figures

Figure 2.1 Strain-time response for HMA mixtures for a static creep test 5
Figure 2.2 Domains of the creep compliance 8
Figure 2.3 Regression constants D_1 and m 9
Figure 2.4 Generalized Maxwell model 10
Figure 2.5 Creep compliances measured at different temperatures (Before construction) 13
Figure 2.6 The creep compliance master curve (After construction) 13
Figure 2.7 The shift factor versus temperature 14
Figure 2.8 Stress and strain during a dynamic modulus test 15
Figure 2.9 Loss and storage modulus 16
Figure 2.10 Estimating fracture temperature (After Hill and Brien, 1966) 23
Figure 2.11 Thermal cracking development mechanism 24
Figure 2.12 Schematic of crack depth model (after Hiltunen and Roque, 1995) 25
Figure 3.1 Sieve analysis for the BM25.0 aggregate 28
Figure 3.2 Sieve analysis for the SM9.5A aggregate 29
Figure 3.3 Sample conditioning chamber and schematic of set up for a uniaxial creep test 31
Figure 3.4 Prior-to-mounting (right) and mounted (left) specimens using a fixture device 31
Figure 3.5 Schematic of environment and set up for an IDT 32
Figure 3.6 Uniaxial creep compliances for the BM25.0 34
Figure 3.7 Uniaxial creep compliances for the SM9.5A 35
Figure 3.8 IDT creep compliances for the BM25.0 35
Figure 3.9 IDT creep compliances for the SM9.5A 36
Figure 4.1 Relationship between shift factor and testing temperatures 38
Figure 4.2 CCMCs of each mix and testing setup 39
Figure 4.3 The Prony series fit with increasing the number of terms 41
Figure 4.4 Prony series models for the uniaxial CCMC 42
Figure 4.5 Prony series models for the IDT CCMC 42
Figure 4.6 Effect of the sigmoidal function coefficients on the CCMC 43
Figure 4.7 Sigmoidal models for the uniaxial CCMC 44
Figure 4.8 Sigmoidal models for the IDT CCMC 45

Figure 4.9 Power models for the uniaxial CCMC 46
Figure 4.10 Power models for the IDT CCMC 47
Figure 4.11 The power model at low temperatures from uniaxial setup 48
Figure 4.12 The power model at low temperatures from IDT setup 48
Figure 4.13 *M*-values for both mixes obtained from the power models 49
Figure 5.1 Storage modulus and sigmoidal fitting curve (BM25.0) 52
Figure 5.2 Predicted relaxation modulus (BM25.0) 52
Figure 5.3 Storage modulus and sigmoidal fitting curve (SM9.5A) 53
Figure 5.4 Predicted relaxation modulus (SM9.5A) 53
Figure 5.5 The relaxation modulus and predicted creep compliance (BM25.0) 54
Figure 5.6 The relaxation modulus and predicted creep compliance (SM9.5A) 55
Figure 5.7 Comparison of the creep compliance predicted from the dynamic modulus and determined in the lab test (BM25.0) 56
Figure 5.8 Comparison of the creep compliance predicted from the dynamic modulus and determined in the lab test (SM9.5A) 56
Figure 5.9 The predicted dynamic modulus (BM25.0) 57
Figure 5.10 The predicted dynamic modulus (SM9.5A) 58
Figure 5.11 Comparison of the predicted and measured dynamic moduli (BM25.0) 58
Figure 5.12 Comparison of predicted and measured dynamic moduli (SM9.5A) 59

List of Tables

Table 3.1 Mixing percentages and material source of BM 25.0 28
Table 3.2 Mixing percentages and material source of SM 9.5A..... 28
Table 3.3 Molded and testing specimen sizes 29
Table 3.4 VTM and G_{mb} for molded specimens 30
Table 3.5 Summary of test specimens for creep analysis..... 30
Table 3.6 Coefficients used to calculate the creep compliance (Kim at el., 2002)..... 33
Table 4.1 Summary of creep compliance shift factors 38
Table 4.2 Regression results: the Prony series fitting..... 41
Table 4.3 Regression results: Sigmoidal function fitting 44
Table 4.4 Regression results: Power function fitting..... 46
Table 4.5 Regression results: Power model at low temperatures..... 49

Chapter 1 Introduction

1.1. Background

When a pavement system is subjected to traffic and/or environmental loading, the stresses induced by the loads produce critical strains in various locations within the pavement system. These critical strains can be used to predict pavement performance. The maximum vertical compressive strains developed in hot-mix asphalt (HMA) layers are used to predict rutting failure. The maximum tensile strains developed at the top and bottom of HMA layer are used to predict thermal and fatigue distresses in the HMA.

Material characterization properties are needed in order to model the pavement and compute the stresses and strains. Flexible pavements are commonly modeled as multilayer linear elastic systems. Thus, the relevant properties are the modulus of elasticity and the Poisson's ratio. However, HMA (a mixture of asphalt binder and aggregate) behaves as a viscoelastic material since its response depends on the temperature and time of loading. Thus, it is important to measure the viscoelastic properties of the material at a wide range of frequencies and temperatures. One of the most common methods for characterizing the response of viscoelastic materials to loading is to measure their creep behavior at different temperatures and times. The various measurements are then shifted using time-temperature superposition to build a creep compliance master curve (CCMC).

The creep test of HMA is of significance because this test makes it possible to determine and separate the time-independent (elastic strain) and time-dependent (viscoelastic and plastic strains) components of the strain response (Witczak et al., 2002). In addition, parameters obtained from creep tests at low temperatures (m-value) are used to predict thermal cracking development and propagation, and those at high temperatures are used to predict rutting in the HMA.

There are two commonly used creep tests: the indirect tensile test (IDT) and the uniaxial compression/tension test. The direct compressive creep test, usually called the uniaxial creep

test, is used to predict permanent deformation (rutting) on the surface of pavement, whereas the IDT is used to characterize HMA mixtures for thermal cracking prediction at low temperatures.

The two creep configurations, IDT and uniaxial creep test for HMA mixtures, were utilized in this research. Test temperature ranged from -15 to 40°C. Two mixes were studied: a surface mix (SM9.5A) and a base mix (BM25.0). These mixtures were part of a Material Characterization Project conducted at the Virginia Tech Transportation Institute (VTTI) (Flintsch et al., 2005). To minimize the effects of sample preparation on the comparison, all the samples were compacted using the same Troxler Gyratory Compactor. Ten samples were prepared for each mix.

1.2. Problem Statement

Two mathematical models have been used to represent CCMC: the Prony series and the power models. The Prony series was used because it has a mechanical analogy and because this model is efficient when a Laplace transformation is used to interconvert various viscoelastic properties. However, finding the most appropriate number of terms and the coefficients of the series may be a tedious and time-consuming exercise even if a statistical package is employed. The power model is simpler and has been extensively used to find the m-value, which measures the mix susceptibility to thermal cracking. However, it can only explain the trend of the creep compliance over a limited range of reduced times.

1.3. Objectives

The main goal of this investigation was to find the most appropriate mathematical models to represent the CCMC obtained from measurements using the two creep test configurations. The two commonly used models (the Prony series and power models) as well as a new model (the sigmoidal function) were studied. Furthermore, the effect of the m-value resulting from the power model on thermal cracking prediction was examined and comparisons among viscoelastic material functions were analyzed using interconversion methods.

1.4. Significance

Finding statistical CCMC models and comparing them convey a fundamental understanding of viscoelastic materials. Additionally, the CCMC mathematical models not only provide a general understanding of how the creep compliance varies over a broad band of reduced times, but also help estimate a particular creep value at a given reduced time. Furthermore, if the interconversion method proves accurate, it can facilitate converting viscoelastic properties such as the creep compliance, relaxation modulus, and dynamic (complex) modulus.

1.5. Research Scope

To accomplish the objective of this research, specimens were tested using IDT and uniaxial configurations. Regression and graphical data analyses were employed to model the material response and compare the results from both tests. Several analytical conversions among viscoelastic properties were also investigated.

This thesis is comprised of six chapters. Chapter 2 presents the background on the creep behavior of asphalt materials, covering creep tests, testing setup, and models to characterize the material. Chapter 3 describes the testing program conducted in the study, including the preparation and mixing of materials, testing equipment, and test protocols. Chapter 4 presents the construction of CCMC, the statistical modeling of the CCMC, and their application to predict thermal cracking at low temperatures. Chapter 5 compares viscoelastic properties predicted through interconversion methods with those measured directly in the lab. Chapter 6 presents the findings and conclusions of the research along with recommendations for future research.

Chapter 2 Literature Review

2.1. Introduction

This chapter reviews the most relevant published reports and papers on the measurement of viscoelastic material properties, such as the creep compliance, relaxation modulus, and dynamic modulus; testing methods to measure these properties; thermal cracking mechanism and models; and interconversion procedures.

2.2. The Creep Compliance

Creep is defined as a time-dependent deformation that occurs when a material is subjected to loading over time. The modulus of a material, which is simply the reciprocal of the compliance, is used to model pavement systems and predict stresses, strains, and distresses (Witczak et al., 2002). However, when considering the viscoelastic behaviour of asphalt materials, it is often more advantageous to use the creep compliance than to use the modulus because the compliance can allow separation of its response over time into time-dependent and time-independent components (Witczak et al., 2002). In a creep test a static load is applied to a specimen and the deformation over time is measured. The creep compliance is then computed using Equation (1).

$$D(t) = \frac{\varepsilon(t)}{\sigma_0} \tag{1}$$

where

$D(t)$ = creep compliance,

t = testing time,

$\varepsilon(t)$ = strain at a given time, and

σ_0 = constant stress.

The typical strain versus time response of HMA on a single load-unload cycle is illustrated in Figure 2.1. This figure shows all the components of the deformation of a viscoelastic material under a static load. The total strain (ε_T) can be divided into recoverable and irrecoverable components, both with time-dependent and time-independent subcomponents as shown in Equation (2). A material with a high creep compliance at a certain time is prone to deform more than a material with a relatively low compliance value at the same time.

$$\varepsilon_T = \varepsilon_e + \varepsilon_p + \varepsilon_{ve} + \varepsilon_{vp} \tag{2}$$

where

ε_T = total strain,

ε_e = elastic strain (recoverable and time-independent),

ε_e = plastic strain (irrecoverable and time-independent),

ε_{ve} = viscoelastic strain (recoverable and time-dependent), and

ε_{vp} = viscoplastic strain (irrecoverable and time-dependent).

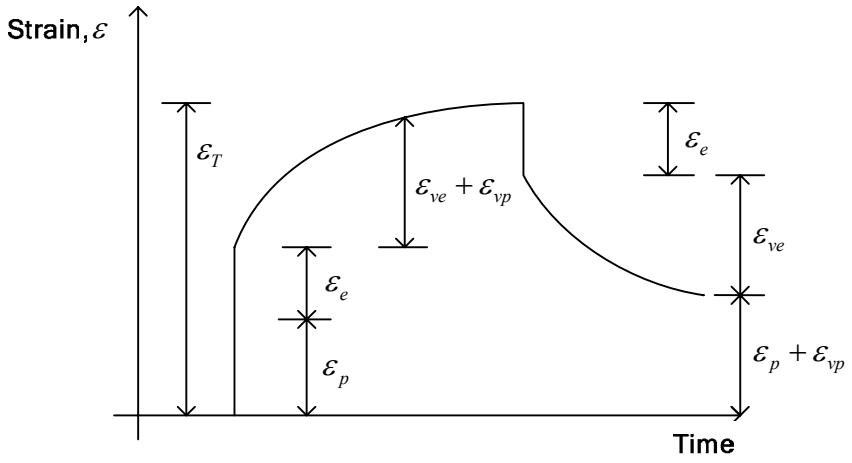

Figure 2.1 Strain-time response for HMA mixtures for a static creep test

2.2.1. Creep Compliance Test Configurations

There are different laboratory testing modes for measuring the creep compliance of HMA: uniaxial, triaxial, or indirect tensile. The uniaxial configuration has traditionally been used to characterize and predict permanent deformation of flexible pavement because the data analysis is simple and the geometry of this test is believed to replicate the asphalt behavior in situ. A detailed review of the uniaxial test is presented in Chapter 3. The triaxial mode of testing is even more representative of in-situ conditions because the horizontal confinement is similar to that in the field. However, the mode is not widely used due to the complexity of setting up the equipment.

Brown and Foo (1994) compared the unconfined and confined uniaxial (triaxial) creep tests and their ability to predict rutting in HMA. As expected, it was found that the unconfined uniaxial creep test was not capable of simulating field conditions because the samples failed when subjected to high stress and temperature. Conversely, confined creep test mimicked field conditions fairly well. It was also found that the air void in the samples was reduced after the unconfined creep test. This is contrasted with phenomenon that occurred in the field. The researchers recommended the use of confined creep tests for characterizing rutting performance.

The indirect tensile (IDT) creep test was chosen by the Strategic Highway Research Program (SHRP) to characterize thermal cracking performance of HMA at low temperatures (Roque et al. 1995). The test is considered the most promising method to predict HMA performance at low temperatures (Christensen et al. 2004). In particular, this test is used to determine a fracture property (the m-value) of HMA at low temperatures. The procedure has been standardized in AASHTO T332 “Standard Method of Test for determining the Creep Compliance and Strength of Hot-Mix Asphalt (HMA) Using the Indirect Tensile Test Device.”

One advantage of the IDT is that it uses a compressive loading method that is applied to a cylindrical specimen to create a uniform state of tensile stress in the perpendicular direction (Roque et al., 1995). It is assumed that the loading alignment is perfect. The indirect tensile creep test measures the horizontal and vertical displacement next to the center of a cylindrical specimen. The measurements are then used to compute the Poison ratio and the creep compliance. The main disadvantage is that the stress and strain distributions are more complex

than those of uniaxial test. The mathematical models used to describe the IDT creep compliance are similar to those used for the uniaxial creep test.

Christensen and Bonaquist (2004) conducted an extensive comparison of HMA creep compliance measurements using different testing setups: uniaxial tension, uniaxial compression, and the IDT. The investigation focused on the following issues:

- Evaluation of the difference between creep compliances determined in tension and compression at low temperatures
- Comparison of the creep compliances measured with in the IDT and uniaxial setups
- Identification of any relationship between the two tests

The creep tests were performed using various types of HMA at three low temperatures (-20, -10, and 0°C) for 100 seconds. The comparison showed that the creep compliances in tension were higher than those in compression. The difference increased at higher temperatures. Similarly, the uniaxial tension creep compliances were higher than those measured using the IDT configuration. However, the researchers pointed out that this discrepancy depends largely on specific aggregate used in asphalt mixtures such as its size and/or orientation. They also observed that the uniaxial compression creep compliances were higher than the IDT compliances: the differences ranged from 8 to 20 percent. The researchers attributed the differences to diverse anisotropy effects in the two tests (e.g., geometry of specimen) and volumetric variations (e.g., different air void distribution).

A typical relationship between the calculated total compliance and loading time is shown in Figure 2.2. The creep compliance curve can be divided into three different parts (Witczak et al., 2002):

- Primary creep: the portion wherein the strain rate decreases with loading time
- Secondary creep: the portion wherein the strain rate is constant with loading time
- Tertiary creep: the portion wherein the strain rate increases with loading time

A large increase in creep compliance occurs within the tertiary part. The point at which tertiary deformation begins is defined as the flow time (F_T). This has been found to be an important parameter in evaluating HMA rutting resistance (Hafez, 1997). The flow time (F_T) is defined as the time at which the shear deformation under constant volume starts (Kim et al., 2002). The

flow time is also regarded as the minimum point of the rate of change for compliance to loading time (Witczak et al., 2002).

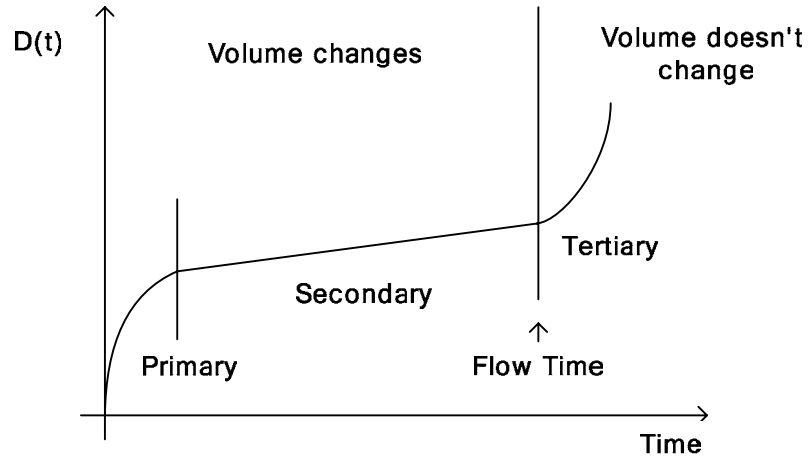

Figure 2.2 Domains of the creep compliance

2.2.2. Creep Compliance Models

The two most commonly used mathematical models for representing the creep compliance master curve (CCMC) are the power function and Prony series. The power models [Equation (3)] are commonly used to analyze the secondary part of the CCMC when plotted on logarithmic space as presented in Figure 2.3 (Kim et al., 2002).

$$D(t) = D_0 + D_1 t^m \tag{3}$$

where

D_0 = instantaneous creep compliance,

$D(t)$ = total creep compliance at any time,

t = loading time, and

D_1, m = materials regression coefficients.

The regression coefficients D_1 and m are commonly referred to as the compliance parameters. The compliance value increases as either the D_1 or m-value increases.

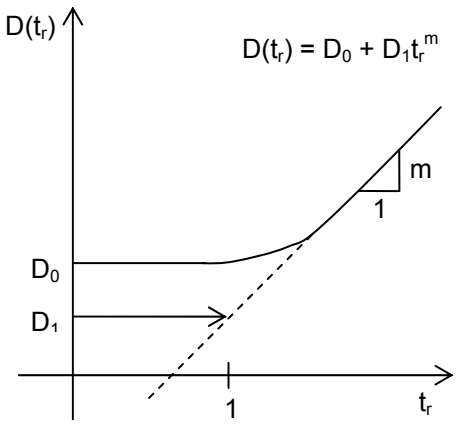

Figure 2.3 Regression constants D_1 and m

The other popular method used to model the creep compliance is the Prony series. This approach uses the generalized Maxwell model analogy (Figure 2.4) to represent the viscoelastic properties of the asphalt concrete mixture in relaxation. Hiltunen and Roque (1995) found that this method is useful to represent the compliance because the Prony series simplifies the interconversion between the creep compliance and relaxation modulus. The Prony series is defined by the following equation:

$$D(t_r) = D_g + \sum_{i=1}^{n} D_i (1 - e^{-t_r/\tau_i}) \qquad (4)$$

where

$D(t_r)$ = creep compliance at reduced time t_r,

$D_g = \lim_{t_r \to 0} D(t_r)$ = equilibrium (glassy) creep compliance,

t_r = reduced time (t/a_T),

a_T = temperature shift factor, and

D_i, τ_i = Prony series parameters.

.

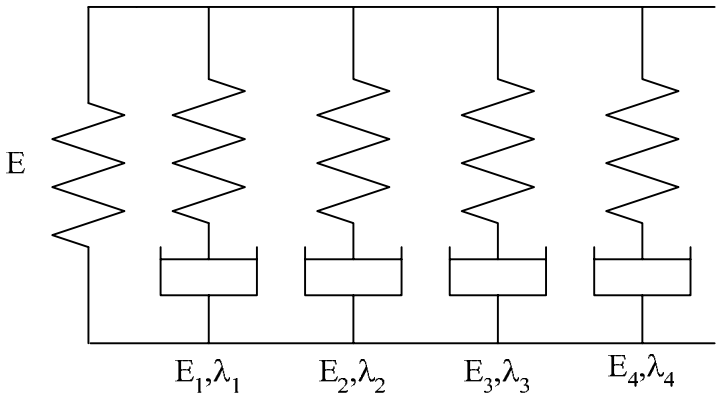

Figure 2.4 Generalized Maxwell model

2.3. The Relaxation Modulus

Stress relaxation of asphalt materials is a phenomenon similar to creep. In the creep test, a constant loading to the material and an instant strain (ε_0) occur causing the material to creep with time. On the other hand, if the instant strain is fixed and remains constant, then the applied stress will be relaxed. This reduction in stress over time is called stress relaxation and the relaxation modulus is computed using Equation (5).

$$E(t) = \frac{\sigma(t)}{\varepsilon_0} \tag{5}$$

where

$E(t)$ = relaxation modulus,

$\sigma(t)$ = stress at any time, and

ε_0 = instantaneous strain.

The relaxation modulus is used to predict thermal stress in asphalt pavements. Thermal stress in the pavement can be computed using the constitutive Equation (6), which explains the stress development during cooling. This equation is based on Boltzmann's superposition principle for linear viscoelastic materials (Hiltunen et al. 1994).

$$\sigma(t_r) = \int_0^{t_r} E(t_r - t_r')\frac{d\varepsilon}{dt_r'}dt_r' \quad (6)$$

where

$\sigma(t_r)$ = stress at reduced time t_r,

$E(t_r - t_r')$ = relaxation modulus at reduced time $t_r - t_r'$,

ε = strain at reduced time t_r, and

t_r' = variable of integration.

Similar to the creep compliance, the relaxation modulus can be modeled using the Prony series (Hiltunen et al. 1994). Representing the relaxation modulus as a Prony series [Equation (7)] depicts the computational efficiency in relation to its decaying exponential function (Park et al. 2001). Furthermore, since all linear viscoelastic properties encode the same information, they can be analytically interconverted without changing their original information (Park et al. 1999). These interconversions are facilitated by the use of the Prony series.

$$E(t_r) = E_e + \sum_{i=1}^{n} E_i e^{-t_r/\lambda_i} \quad (7)$$

where

$E(t_r)$ = relaxation modulus at reduced time t_r,

$E_e = \lim_{t_r \to 0} E(t_r)$ equilibrium relaxation modulus,

E_i = Prony series parameters for the relaxation modulus master curve in Maxwell model, and

λ_i = relaxation time.

The time and temperature dependent relaxation modulus is needed to calculate thermal stress at a particular point in time. Ideally, the relaxation modulus could be obtained from a laboratory test. However, this test is not widely used because it is relatively difficult to perform. Instead, the modulus can be obtained from a CCMC using interconversion. This can be done using an exact method based on the convolution integration, or approximated methods. Interconversion methods between viscoelastic properties are discussed in Section 2.7.

2.4. Time-Temperature Superposition and Master Curve

The response dependence on both time and temperature is evaluated for the characterization of viscoelastic materials such as HMA. In general, creep tests are performed at various temperatures. However, the time and temperature dependent creep response can be expressed by a single parameter, reduced time (t_r), using the time-temperature superposition principle (Painter and Coleman, 1997). Data collected at different temperatures, -15, 5, 20, 30, and 40˚C in this study, can be shifted to form a CCMC at a reference temperature (usually 20˚C). The amount of shifting required at each temperature is called the shift factor, $a(T)$, and is a constant by which the loading times at each temperature can be divided to give a reduced loading time, t_r, for the master curve. The reduced time is calculated using the following Equation:

$$t_r = \frac{t}{a(T)} \tag{8}$$

where

t_r = reduced time of loading,

t = actual time of loading, and

$a(T)$ = shift factor for data measured at temperature (T).

Creep compliances measured at temperatures below the reference temperature should be shifted toward the left direction to construct a single smooth line of master curve as shown in Figure 2.5 and Figure 2.6. This is because compliance values at temperatures lower than the reference temperature should be lower than those at higher temperatures and vice versa. Figure 2.7 shows a typical relationship between the shift factor and temperatures on a semi-log plot (from Figure 2.5 and Figure 2.6).

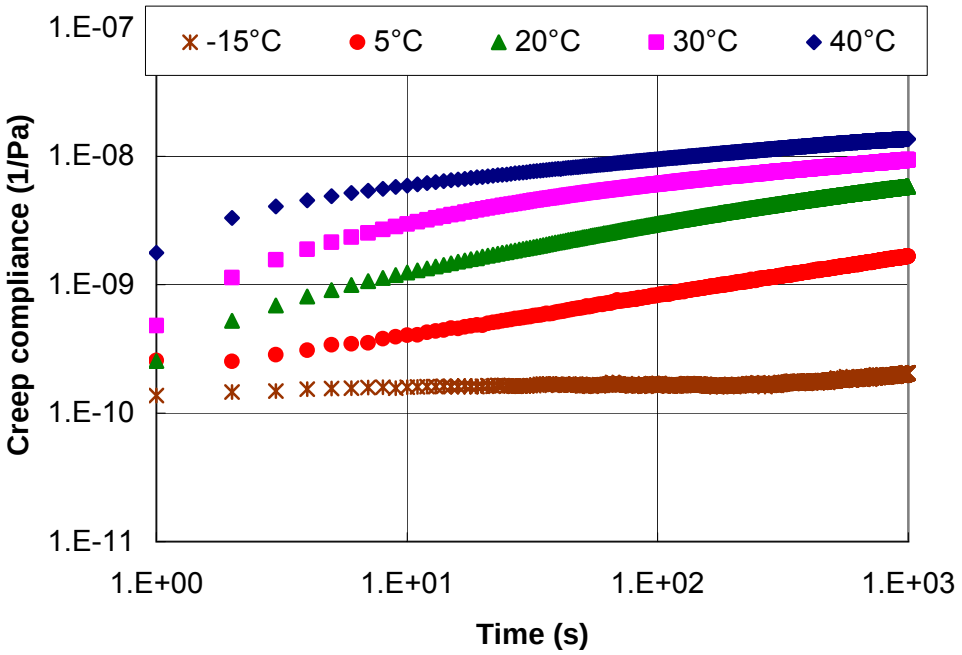

Figure 2.5 Creep compliances measured at different temperatures (Before construction)

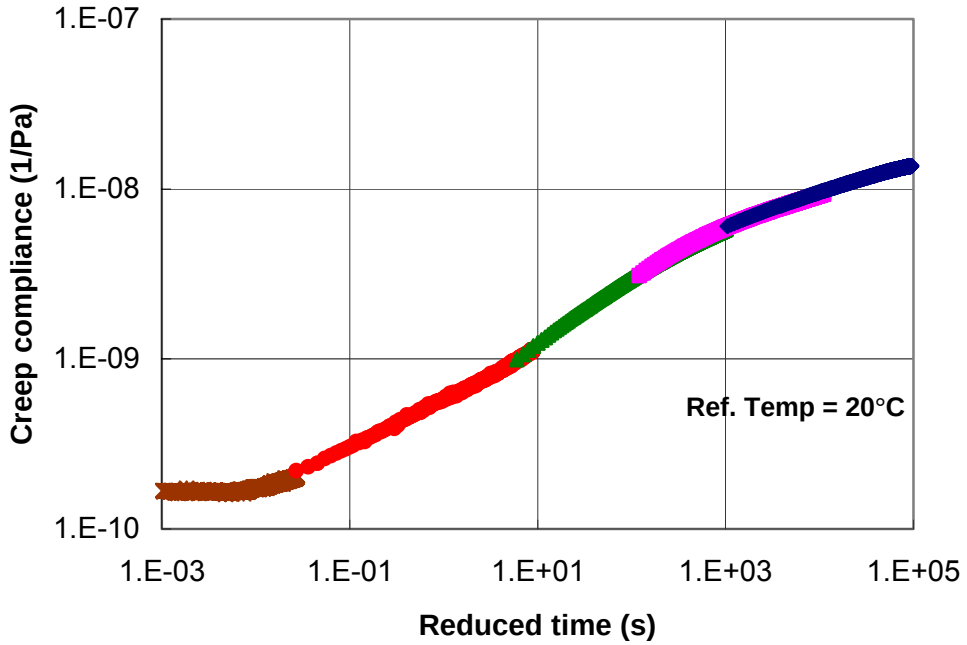

Figure 2.6 The creep compliance master curve (After construction)

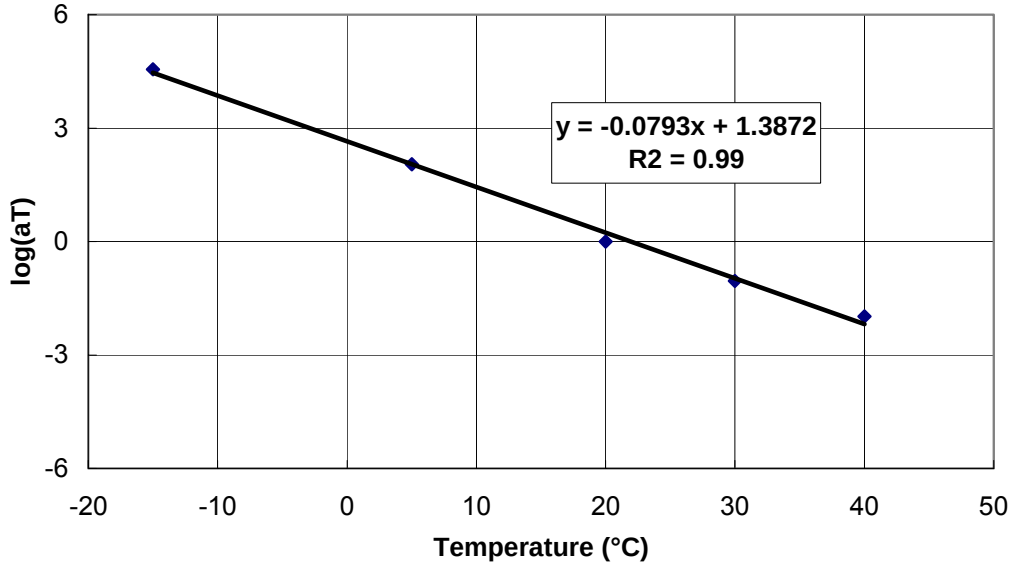

Figure 2.7 The shift factor versus temperature

2.5. Dynamic (Complex) Modulus

The dynamic (complex) modulus (E*) is another important viscoelastic property used for characterizing HMA. It can be determined in the lab by applying steady-state sinusoidal loading to asphalt specimens at different frequencies. The applied stress and corresponding strain response are measured, and the dynamic modulus is calculated using Equation (9). Figure 2.8 shows typical stress and strain curves for a dynamic modulus test, which are defined by Equations (10) and (11), respectively.

$$|E^*| = \frac{\sigma_0}{\varepsilon_0} \tag{9}$$

$$\sigma = \sigma_0 \sin(\omega t) \tag{10}$$

$$\varepsilon = \varepsilon_0 \sin(\omega t - \phi) \tag{11}$$

where

σ_0 = applied steady state stress amplitude,

ε_0 = measured strain amplitude,

ω = angular frequency ($2\pi f$, where f = frequency), and

ϕ = phase angle in radians ($\omega\Delta t$, where Δt = time lag between stress and strain).

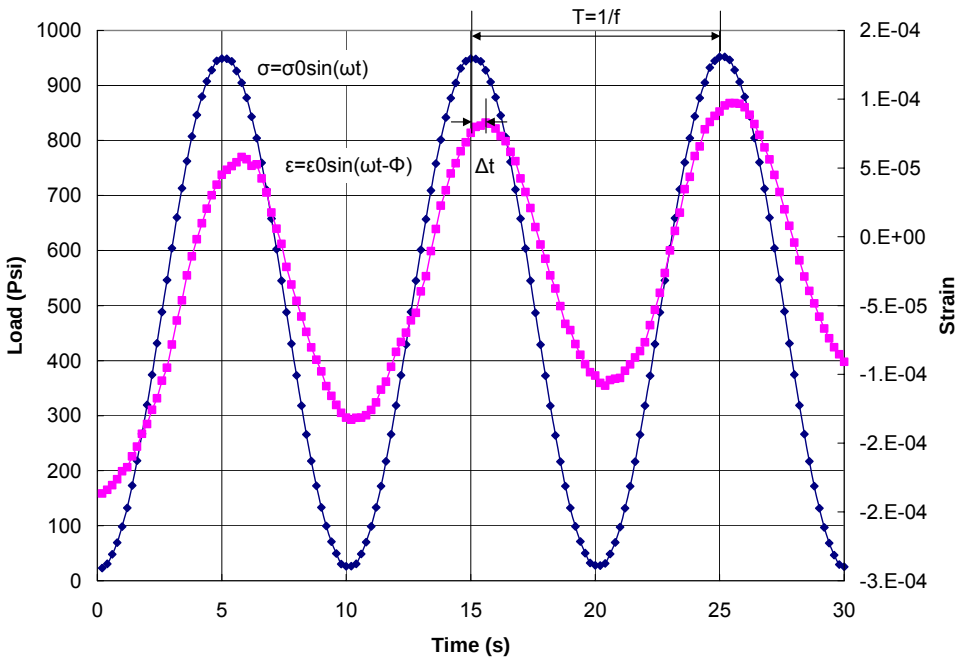

Figure 2.8 Stress and strain during a dynamic modulus test

Two parameters are determined in a dynamic modulus test: the dynamic modulus and phase angle (ϕ). The phase angle gives an indication of how viscous the material is; the material becomes more viscous as the phase angle increases. For example, if the phase angle is zero, the material behaves as purely elastic. A phase angle of 90 degree means that the material behaves as purely viscous.

To be able to characterize the behavior of the material over a wide range of temperatures and frequencies, the dynamic modulus is measured at different temperatures. The curves are then shifted using time-temperature superposition to produce a dynamic modulus master curve.

The complex modulus is represented by a complex number [Equation (12)], consisting of a real (storage) part (E') and an imaginary (loss) part (E"). These components (Figure 2.9) account for the elastic and viscous behavior of the material, respectively, and they can be computed using Equations (13) and (14).

$$E^* = E' + iE'' \quad (12)$$

$$E' = |E^*| \cos(\phi) \quad (13)$$

$$E'' = |E^*| \sin(\phi) \quad (14)$$

where

E' = real part of the dynamic modulus (storage modulus),

E" = imaginary part of the dynamic modulus (loss modulus), and

$i = \sqrt{-1}$.

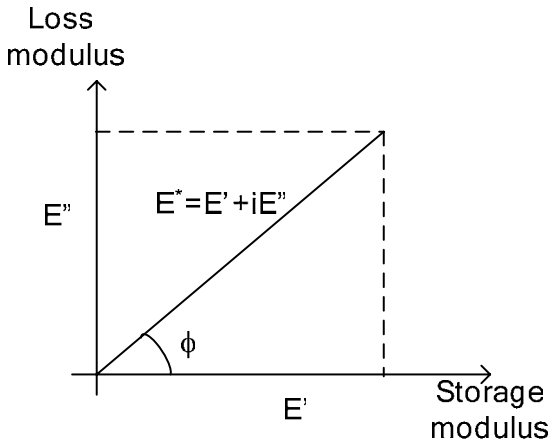

Figure 2.9 Loss and storage modulus

Witczak (2000) proposed an equation to predict the dynamic modulus based on the mix volumetric properties. Equation (15) can be used to predict the dynamic modulus over a wide range of frequencies and temperatures based on binder viscosity and HMA volumetric design properties, which are readily available, rather than conducting the dynamic modulus test in the lab. The equation had a coefficient of determination (R^2) of 96% for the 205 mixes evaluated. Other studies confirmed the appropriateness of the model (Witczak et al., 2000).

$$\log E^* = 3.750063 + 0.02932\rho_{200} - 0.001767(\rho_{200})^2 - 0.002841\rho_4 - 0.058097V_a$$
$$-0.802208\left(\frac{V_{beff}}{V_{beff}+V_a}\right) + \frac{3.871977 - 0.0021\rho_4 + 0.003958\rho_{38} - 0.000017(\rho_{38})^2 + 0.005470\rho_{34}}{1 + e^{(-0.603313 - 0.313351\log(f) - 0.393532\log(\eta))}} \quad (15)$$

where

E^* = dynamic modulus in psi,

η = bitumen viscosity in 10^6 Poise,

f = loading frequency in Hertz,

V_a = air void content in percent,

V_{beff} = effective bitumen content in percent,

ρ_{34} = cumulative percent retained on the ¾ in sieve,

ρ_{38} = cumulative percent retained on the 3/8 in sieve,

ρ_4 = cumulative percent retained on the No. 4 in sieve, and

ρ_{200} = percent passing the No. 200 sieve.

2.6. Sigmoidal Functions for Modeling Mater Curves

Pellinen and Witczak (2002) proposed using a sigmoidal function [Equation (16)] for modeling the dynamic modulus master curve. The sigmoidal function is fitted to the dynamic modulus test data using regression analysis.

$$\log|E^*| = \delta + \frac{\alpha}{1 + e^{\beta - \gamma \log f_r}} \tag{16}$$

where

log $|E^*|$ = log of the dynamic modulus,

f_r = reduced frequency, and

α, β, γ, δ = fitting parameters.

This fitting function provides an analytically simple form that can be used to easily determine the physical characteristics of a material at any temperature and loading time. Furthermore, the equation parameters are of significance because they encode some meaningful information. The parameters α and $\alpha+\delta$ represent the minimum and maximum dynamic modulus values, respectively. For example, the maximum dynamic modulus ($\alpha+\delta$) represents the maximum stiffness of asphalt mixture, which at high temperature relies mainly on aggregate interlock, but

at intermediate and low temperatures depends also on the binder stiffness. The parameters β and γ describe the shape of the sigmoidal function (Pellinen et al. 2002).

2.7. Interconversion among Viscoelastic Material Properties

Linear viscoelastic material properties (i.e., the creep compliance, relaxation modulus, complex compliance, and dynamic modulus) can be converted to each other analytically because they encode fundamentally the same information (Kim et al. 2002). This philosophy makes it possible to predict one viscoelastic property from another. For instance, if the relaxation modulus is needed but it is difficult to measure directly from a test, it would be convenient to predict it from another viscoelastic property such as the creep compliance or dynamic modulus through appropriate interconversion method (Schapery et al. 1999).

2.7.1. Interconversion between the Relaxation Modulus and Creep Compliance

Ferry (1980) showed that there is an exact relationship between the creep compliance and relaxation modulus by using the convolution integral in Equation (17).

$$\int_0^t E(t-\tau)D(\tau)d\tau = t \quad \text{for t>0} \tag{17}$$

where
$E(t)$ = relaxation modulus,
$D(t)$ = creep compliance,
t = time, and
τ = integral variable.

When an analytical form of a viscoelastic material is not available and only data points determined in the laboratory exist, the integral can be solved numerically (Park et al., 1999). However, the numerical method requires significantly tedious and cumbersome work. For this reason, researchers have proposed several approximate methods to convert linear viscoelastic properties to each other. The simplest and crudest method is the quasi-elastic approximation

presented in Equation (18). Generally, this method is not applicable for typical viscoelastic materials.

$$E(t)D(t) \cong 1 \text{, for t>0} \tag{18}$$

Another approximate method can be used if both the creep compliance and relaxation modulus are modeled using a power law analytical form. This method is based on Equation (19), which was first proposed by Leaderman (1958). If the compliance and modulus can be expressed by a power law model, which is drawn as a straight line on a logarithmic scale, then their relation is simplified by the Laplace transformation. This transformation is capable of changing the integral form of linear viscoelastic function into an algebraic form in the Laplace domain. It is noteworthy that the exponent *n* of the power law model is the slope of the curve in the logarithmic plot. A zero slope *n* indicates a material is purely elastic since there is no imaginary component.

$$E(t)D(t) = \frac{\sin n\pi}{n\pi} \tag{19}$$

where

$E(t) = E_1 t^{-n}$ and

$D(t) = D_1 t^{n}$.

Practically, lab-determined data are not exactly represented by the power law function. However, if the data does not perfectly follow a power model but the functions behave smoothly, Equation (19) still works well. In this case, the local slope of the power model can be determined using Equation (20) (Park et al. 1999). *E*(t) is interchangeable with *D*(*t*).

$$n = \left| \frac{d \log E(t)}{d \log t} \right| \tag{20}$$

2.7.2. Interconversion between the Relaxation Modulus / Creep Compliance and Dynamic Modulus

Schapery and Park (1999) established analytical interconversion methods for linear viscoelastic material properties using the Prony series. The researchers showed that if the time-dependent functions are represented by the Prony series as in Equation (4) or (7), they can be analytically converted into frequency-dependent functions (e.g., the dynamic modulus) using Equations (21) through (24):

$$E'(\omega) = E_e + \sum_{i=1}^{m} \frac{\omega^2 \lambda_i^2 E_i}{\omega^2 \lambda_i^2 + 1} \quad (21)$$

$$E''(\omega) = \sum_{i=1}^{m} \frac{\omega^2 \lambda_i^2 E_i}{\omega^2 \lambda_i^2 + 1} \quad (22)$$

$$D'(\omega) = D_g + \sum_{j=1}^{n} \frac{D_j}{\omega^2 \tau_j^2 + 1} \quad (23)$$

$$D''(\omega) = \sum_{j=1}^{n} \frac{\omega \tau_j D_j}{\omega^2 \tau_j^2 + 1} \quad (24)$$

where

ω = angular frequency ($2\pi f$),

$E_e = \lim_{t_r \to 0} E(t_r)$ equilibrium relaxation modulus,

E_i, λ_i = Prony series parameters,

$D_g = \lim_{t_r \to 0} D(t_r)$ equilibrium (glassy) creep compliance, and

D_i, τ_i = Prony series parameters.

For instance, if one has a set of lab-determined creep compliance data under transient loading and it is represented by the Prony series, *D'(ω)* and *D"(ω)* are obtained through the relationship expressed in Equations (23) and (24). Then, frequency dependent viscoelastic properties, both the complex compliance (*D**) and dynamic modulus (*E**), can be determined as follows:

$$D^*(\omega) = D'(\omega) - iD''(\omega) \tag{25}$$

$$\left|D^*(\omega)\right| = \sqrt{\left(D'(\omega)\right)^2 + \left(D''(\omega)\right)^2} \tag{26}$$

$$E^*(\omega)D^*(\omega) = 1 \tag{27}$$

Schapery and Park (1999) also proposed approximate interconversion methods and verified them using polymeric material represented by the Prony series. Equations (28) and (29) show the formulas to convert between the dynamic modulus and relaxation modulus. These relationships were derived based on the assumption that the time-dependent material is represented by the power model (e.g., $E(t) = E_1 t^{-n}$). Therefore, if the source function can be expressed by the power model, the method produces exact results. However, they can also be used to produce an approximate solution using the slope of the curves at each point. This is the same philosophy used for the approximate interconversion between the relaxation modulus and creep compliance described in the previous section.

$$E'(\omega) \cong \lambda' E(t)\Big|_{t=(1/\omega)} \text{ or } E(t) \cong \frac{1}{\lambda'} E'(\omega)\Big|_{\omega=(1/t)} \tag{28}$$

$$E''(\omega) \cong \lambda'' E(t)\Big|_{t=(1/\omega)} \text{ or } E(t) \cong \frac{1}{\lambda''} E''(\omega)\Big|_{\omega=(1/t)} \tag{29}$$

where

λ' = adjust function ($\Gamma(1-n)\cos(n\pi/2)$),

λ'' = adjust function ($\Gamma(1-n)\sin(n\pi/2)$),

Γ = gamma function ($\Gamma(n) = \int_0^\infty u^{n-1}e^{-u}du$), and

n = the local log-log slope of the storage modulus $\left(\left|\frac{d\log E'(\omega)}{d\log\omega}\right|\right)$.

2.8. Thermal Cracking Models

Several models have been proposed to predict thermal cracking on flexible pavements. In general, they can be categorized into two groups: empirical-based models and mechanistic-

based models. The empirical models have been developed using statistical analyses, such as the regression method, while the mechanistic models are based on the mechanics of materials (Marasteanu et al., 2004).

2.8.1. Empirical-based Models for Thermal Cracking on Flexible Pavement

Most available empirical models were developed based on limited databases, thus, the regression models often have low reliability. However, they allow determination of which pavement characteristics have a significant effect on thermal cracking (Marasteanu et al., 2004). A few examples are discussed below.

Fromm and Phang (1972) developed an empirical model to predict a cracking index based on HMA, pavement and climate variables. The cracking index, used by the Ontario Department of Transportation, evaluates the cracking severity based upon the number of transverse cracks. Researchers measured the number and severity of cracks in 33 locations in Ontario, Canada and developed transverse cracking prediction models using step-wise linear regression analysis. They initially considered 40 variables; however, variables that did not have a significant effect on the crack index were eliminated. Nine and eleven variables for general/southern and northern models, respectively, were chosen to express the thermal cracking phenomenon. The coefficient of determination (R^2) for the models ranged from 0.64 to 0.70.

Hass et al. (1987) collected thermal cracking data, pavement characteristics and climatic parameters at 25 airports in Canada and developed equations to predict the average spacing between thermal cracks through step-wise statistical analyses. They concluded that low temperature cracking at the airports depends largely on the influence of asphalt binder characteristics in terms of PVN (McLeod's Pen-Vis Number) or asphalt mixture characteristics such as layer thickness and minimum temperature experienced. They also found that the PVN values examined in their study ranged from 0.2 to -1.7. This was almost the same range for unaged asphalt commonly used in Canada. The McLeod's PVN is a correlation between asphalt cement and the temperature susceptibility of the asphalt (McLeod, 1972).

2.8.2. Mechanistic-based Models

Researchers have also investigated the prediction of thermal cracking using mechanistic principles. Although the mechanistic prediction models for the computation of thermal cracking are more complicated than the empirical ones, they deal with the cracking phenomenon at a more fundamental level.

Hills and Brien (1966) first predicted the temperatures at which thermal cracks occur on the surface of pavements. This study was based on the elastic behavior of asphalt material at low temperatures. The researchers asserted that the fracture would occur when thermal stress and thermal strength curves intercept (Figure 2.10). The thermal strength line assumes that tensile strength of HMA is a function of its stiffness, citing Heukelom's (1966) work. The researchers assumed that the pavement behaves as an infinite beam or slab in order to calculate the thermal stresses.

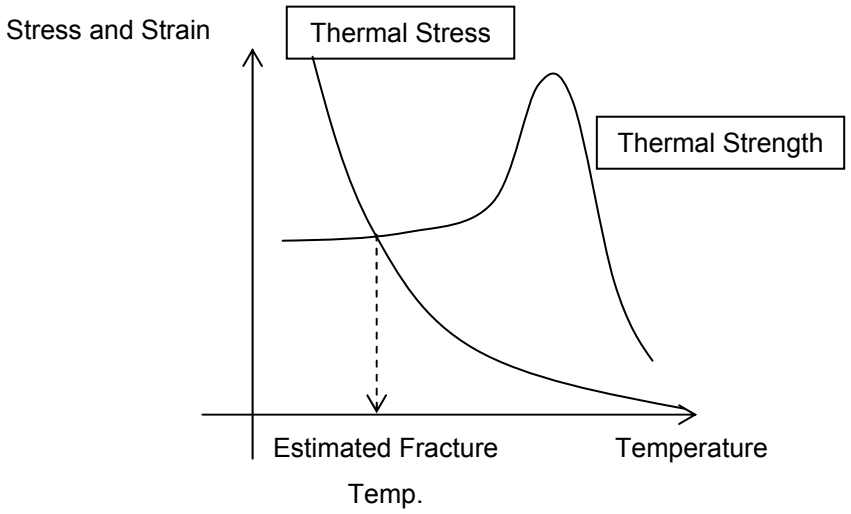

Figure 2.10 Estimating fracture temperature (After Hill and Brien, 1966)

Christison et al. (1972) employed five models to compare predicted and measured fracture temperatures: Pseudo-elastic beam, approximate pseudo-elastic slab, viscoelastic beam, viscoelastic slab, and approximate viscoelastic slab. Real field data was obtained from two test roads constructed in Alberta and Manitoba, Canada in 1966 and 1967, respectively. The field data provided a solid foundation to evaluate the considered stress predictive methods. The data

from the test roads suggested that a suitable pseudo-elastic beam analysis produces reasonable results.

NCHRP Report 291 “Development of Pavement Structural Subsystems” (Finn et al., 1986) produced a computer program named COLD (Computation of Low-Temperature Damage) to predict when thermal cracking is likely to occur under known conditions such as temperature, binder and layer thickness. The primary features of the program are the following:

- Temperature computation throughout the pavement structure
- Thermal stress computation on the surface of the asphalt pavement
- Comparison of tensile strength with thermal stress to predict thermal cracking

2.8.3. M-E Design Guide Model (2002)

As part of the SHRP A-005 contract, a new prediction model for thermal cracking over time was developed (Witczak et al., 2000). The new method, which is called TCMODEL, uses mixture properties measured from the IDT creep. Hiltunen and Roque (1995) described the primary thermal cracking mechanism as presented in Figure 2.11:

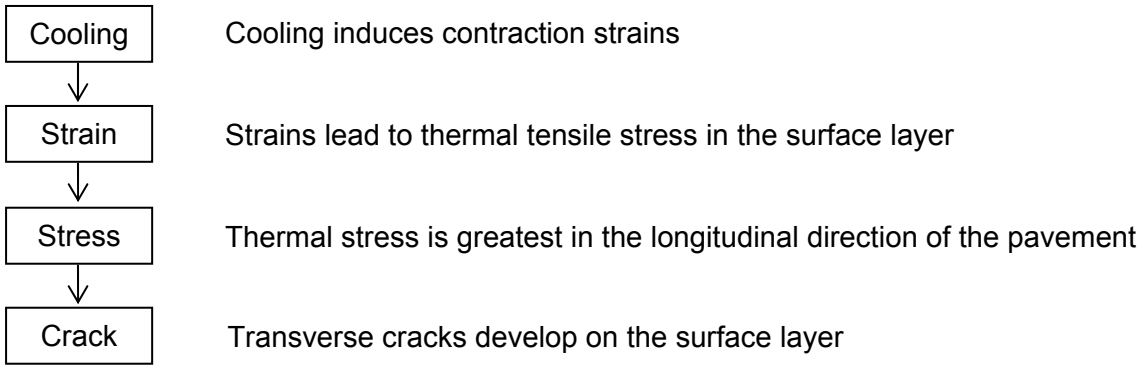

Figure 2.11 Thermal cracking development mechanism

Since pavement temperature is lowest on the surface, there is a high probability that the tensile stress would be maximal on the surface. Therefore, thermal cracking induced by temperature should occur on the surface first. The thermal cracking model proposed by Hiltunen and Roque has two primary components: (1) a mechanistic-based model that computes the propagation of

each crack on a certain area of the surface, and (2) a probabilistic approach to compute the gross amount of thermal cracks. Only the mechanistic-based model will be reviewed herein. Linear elastic fracture mechanics were used to predict crack depth. The fracture model is shown schematically in Figure 2.12. The change in the depth of thermal crack due to the cooling cycle is computed using the Paris relationship presented in Equation (30).

$$\Delta C = A(\Delta K)^n \tag{30}$$

where

ΔC = change in crack depth due to a cooling cycle,

ΔK = change in stress intensity factor due to a cooling cycle, and

A and n = empirically determined fracture parameters.

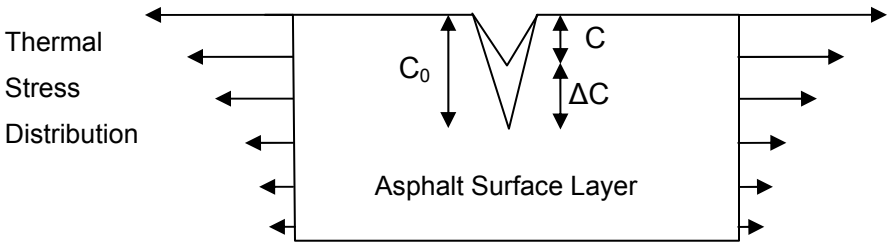

Figure 2.12 Schematic of crack depth model (after Hiltunen and Roque, 1995)

The parameter A can be determined using Equation (31), originally developed by Molenaar (1983) and modified by Witczak et al. (2000). According to the hierarchical levels, the values of 5, 1.5, and 3 are recommended for the levels 1, 2, and 3 (Witczak et al., 2000), respectively.

$$\log A = \beta\left(4.389 - 2.52 * \log(E * \sigma_m * n)\right) \tag{31}$$

where

β = calibration parameter (5, 1.5 or 3 according to the hierarchical level),

E = mixture stiffness = 10000,

σ_m = undamaged mixture tensile strength, and

n = empirically determined fracture parameter.

The researchers recommend measuring the undamaged mixture tensile strength (σ_m) at -10°C. The strength of an asphalt mixture increases with the decrease of temperature. However, below a certain temperature, the strength starts to decrease because the mixture is damaged due to excessive thermal stress. According to tensile tests using cored samples from the field, the maximum tensile strength was usually below -10°C. However, for a conservative design, the strength at -10°C is used to calculate the parameter *A* (Witczak et al., 2000).

Lytton et al. (1983) developed the following relationship to compute the *n*-value based on the *m*-value obtained from modeling the linear part of a creep compliance test with a power model as in Equation (3).

$$n = 0.8\left(1 + \frac{1}{m}\right) \tag{32}$$

where

m = the slope of the linear portion of the CCMC on a logarithmic scale.

Chapter 3 Experimental Program

3.1. Introduction

This chapter describes the experimental program conducted to achieve the objective of this research. The discussion covers sample preparation, conditioning procedure, and creep tests performed. Two sets of creep tests were conducted using uniaxial and indirect tensile creep configurations. MTS and Interlaken servo-hydraulic machines were used to obtain creep data for the IDT and uniaxial test, respectively. Both machines have environmental chambers to constantly maintain a certain temperature.

3.2. Sample Preparation and Conditioning

The specimens were prepared at the VTTI asphalt laboratory. Two typical Virginia mixes were used: a surface mix (SM 9.5A) and a base mix (BM 25.0). The mixes were designed according to VDOT specifications (Flintsch et al., 2005). The mix design for the base course included limestone aggregate, concrete sand, reclaimed asphalt pavement (RAP) and PG 64-22 asphalt binder. The mix design for the surface course used quartzite aggregate, concrete sand, RAP, and the same binder. The job mix formula (JMF) specified by VDOT and the source of the aggregates for both mixes are shown in Table 3.1 and Table 3.2.

Three different samples with the same gradations were prepared for each mix using the percentages presented. Sieve analysis in accordance with AASHTO T27 and T11 was conducted in order to verify whether or not the gradations were acceptable. All the samples met the gradation specifications limits. Figure 3.1 and Figure 3.2 show the 0.45 power gradations for the BM25.0 and SM9.5A, respectively. The triangle marks indicate the upper and lower limits according to the corresponding SUPERPAVE specifications.

Table 3.1 Mixing percentages and material source of BM 25.0

Percentage (%)	Materials: Type	Source	Location
18	#367 Limestone	Acco Stone Co.	Blacksburg, VA
30	#88 Limestone	Acco Stone Co.	Blacksburg, VA
27	#10 Limestone	Acco Stone Co.	Blacksburg, VA
10	Concrete Sand	Wythe Stone Co.	Wytheville, VA
15	RAP	Asams Construction Co.	Blacksburg, VA
4.7	PG 64-22	Associated Asphalt Co.	Roanoke, VA
0.5	Adhere HP+	ARR-MAZ Products	Winter Haven, FL

Table 3.2 Mixing percentages and material source of SM 9.5A

Percentage (%)	Materials: Type	Source	Location
45	#5 Quartzite	Salem Stone Co.	Sylvatus, VA
25	#10 Quartzite	Salem Stone Co.	Sylvatus, VA
15	Concrete Sand	Wythe Stone Co.	Wytheville, VA
15	RAP	Adams Construction Co.	Blacksburg, VA
5.5	PG 64-22	Associated Asphalt Co.	Roanoke, VA
0.5	Adhere HP+	ARR-MAZ Products	Winter Haven, FL

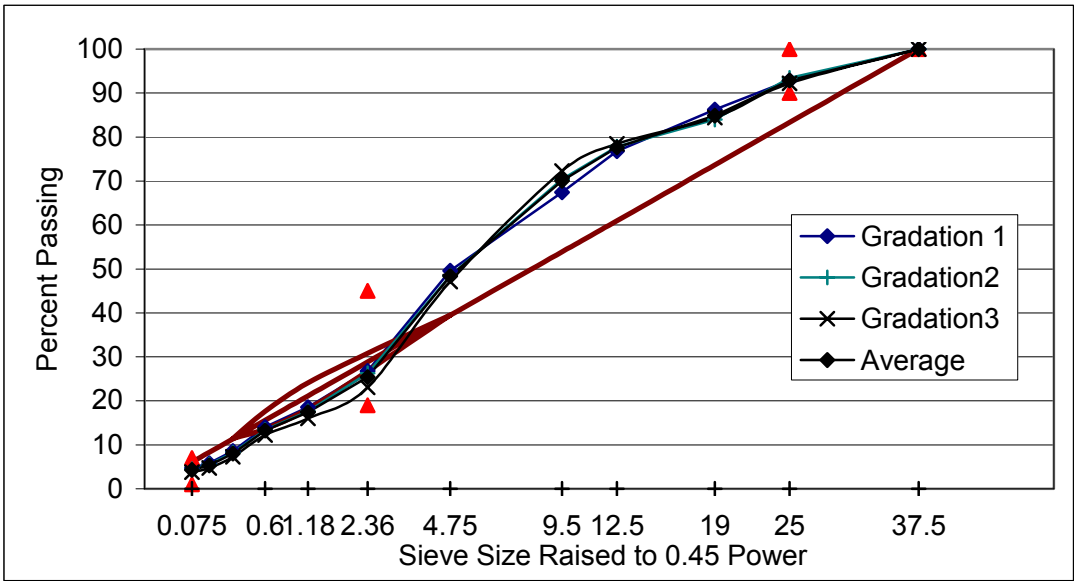

Figure 3.1 Sieve analysis for the BM25.0 aggregate

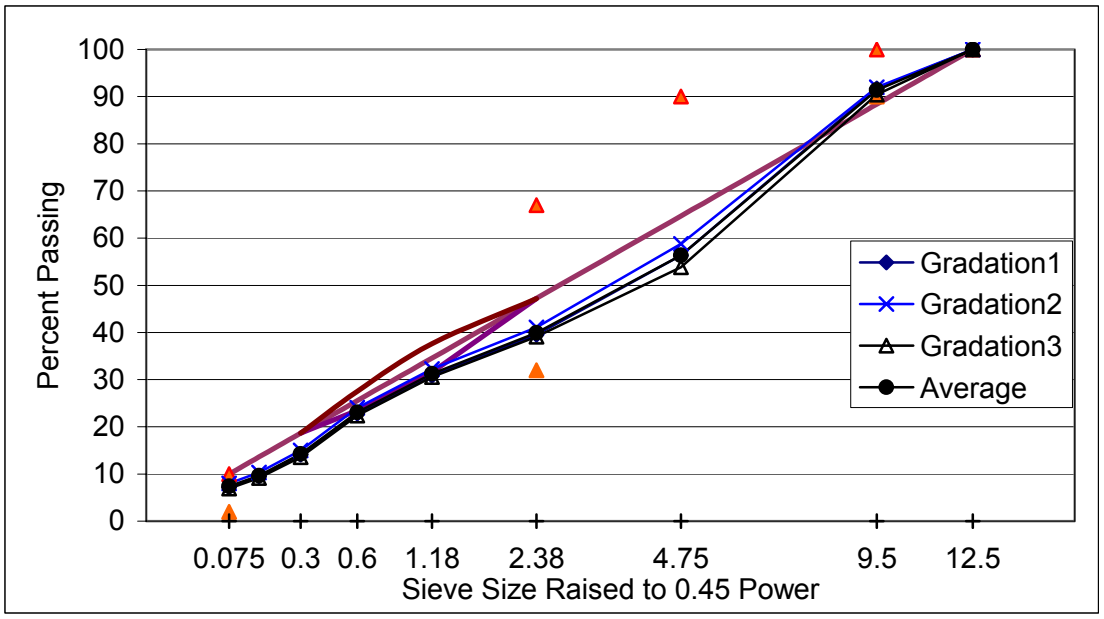

Figure 3.2 Sieve analysis for the SM9.5A aggregate

The SM9.5A IDT specimens were 100mm in diameter by 50mm in height; they were cut from compacted specimens 125mm in thickness. The BM25.0 IDT specimens were 150mm in diameter by 75mm in thickness cut from 150mm by 100mm molded cylinders. For the uniaxial creep and dynamic modulus tests, the specimens were 100mm in diameter by 150mm in height and were cored from 150mm by 178mm compacted specimens. A summary of the specimen's sizes is presented in Table 3.3.

Table 3.3 Molded and testing specimen sizes

Test	SM9.5A		BM25.0	
	Molded Size, mm (in.)	Final Size, mm (in.)	Molded Size, mm (in.)	Final Size, mm (in.)
IDT setup	100X125 (4X5)	100X50 (4X2)	150X100 (6X4)	150X75 (6X3)
Uniaxial setup	150X178 (6X7)	100X150 (4X6)	150X178 (6X7)	100X150 (4X6)

All samples used in this study were compacted using a Troxler Gyratory Compactor (TGC). The specimens were compacted at 65 gyrations as specified by VDOT. The molded SM9.5A specimens were tested using the CoreLok procedure (Instro Tek, 2003) to measure the bulk specific gravity (G_{mb}) of the specimens; the average G_{mb} value was 2.377. The G_{mb} of BM25.0 was measured in accordance with AASHTO T166 and the average G_{mb} value was 2.440. The

maximum theoretical specific gravity (G_{mm}) for both mixes was determined in accordance with AASHTO T209; the average of the G_{mm} were 2.467 and 2.601 for the SM and BM, respectively.

The specimens for the dynamic modulus and uniaxial creep tests were not compacted using a fixed number of gyrations. The specimen weight for the specified testing size (6 in X 7 in) with 4% of air voids was calculated from the measured G_{mm} values and the specimens were compacted using a variable number of gyrations until reaching the required height. The average measured values of G_{mb} and VTM(%) for all specimens used in this research are presented in Table 3.4. It must be noted that these values are for the molded specimens rather than for the cored specimens; which are usually slightly different. Two specimens were tested at each temperature to measure the variability among tested specimens. The testing conditions and sample numbering are summarized in Table 3.5.

Table 3.4 VTM and G_{mb} for molded specimens

Test type	VTM (%)		G_{mb}	
	SM	BM	SM	BM
Dynamic Modulus	4.2	5.0	2.365	2.365
Uniaxial Creep	4.3	5.1	2.365	2.365
IDT Creep	3.6	6.2	2.377	2.440

Table 3.5 Summary of test specimens for creep analysis

Test	Mix	Temperature (°C)				
		-15	5	20	30	40
Uniaxial	SM	S109	S110	S113	S114	S117
		S111	S112	S115	S116	S119
	BM	B78	B79	B60	B61	B55
		B81	B80	B84	B85	B58
IDT	SM	S59	S60	S61	S62	S63
		S66	S67	S68	S69	S70
	BM	B31	B32	B33	B35	B36
		B34	B37	B40	B38	B41
Dynamic Modulus	SM	S93	S94	S97	S98	S105
		S95	S96	S101	S102	S107
	BM	B62	B63	B68	B69	B56
		B64	B65	B76	B77	B67

3.3. Test Methods

3.3.1. Uniaxial Creep Test

In the uniaxial creep test, the strain-time relationship was measured in an unconfined condition. The set-up for the uniaxial creep testing is shown in Figure 3.3. An environmental chamber maintains the samples at a certain temperature to an accuracy of ±0.5˚C. Before the test is performed, samples are conditioned in the chamber for three hours in order to stabilize the temperature. Mounting pucks for three axial extensometers are attached to the side of the specimen with epoxy using a given fixture device (Figure 3.4). A constant stress of 690KPa (100psi) is applied for 1000 sec and the axial deformation and applied load are measured and recorded by the data acquisition system. The testing is performed at -15, 5, 20, 30, and 40˚C.

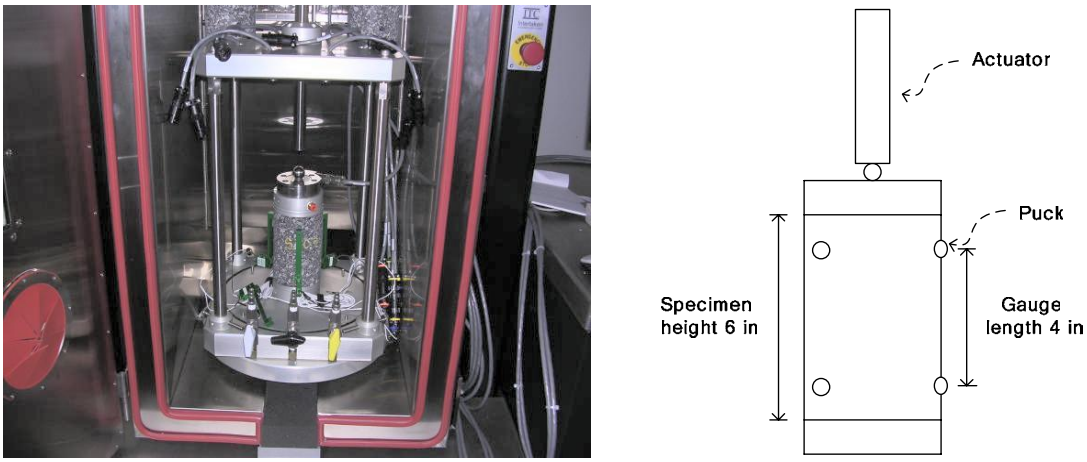

Figure 3.3 Sample conditioning chamber and schematic of set up for a uniaxial creep test

Figure 3.4 Prior-to-mounting (right) and mounted (left) specimens using a fixture device

The computer system automatically computes the average axial deformation by averaging the readings from the three LVDTs. The average deformation values are converted to total axial strain by dividing by the gauge length. (L = 4 in). The total axial compliance [*D(t)*] is then calculated using Equation (1). The total axial compliance over time is plotted in a logarithmic scale.

3.3.2. Indirect Tensile Creep Test

The indirect creep test used in the study is also a single load-unload cycle in which a constant static load is applied to the specimen for 1,000 sec. However, the load is applied diametrically. The pucks for mounting the extensometers are attached on the front and back sides of specimens using an epoxy adhesive. Samples are conditioned in an environmental chamber at the test temperature prior to testing. A constant load, different for each temperature, is applied on the specimens. Horizontal and vertical extensometers measure and record the deformations under the static load. The environmental chamber for the IDT is shown in Figure 3.5, which also shows a typical setup for IDT creep test.

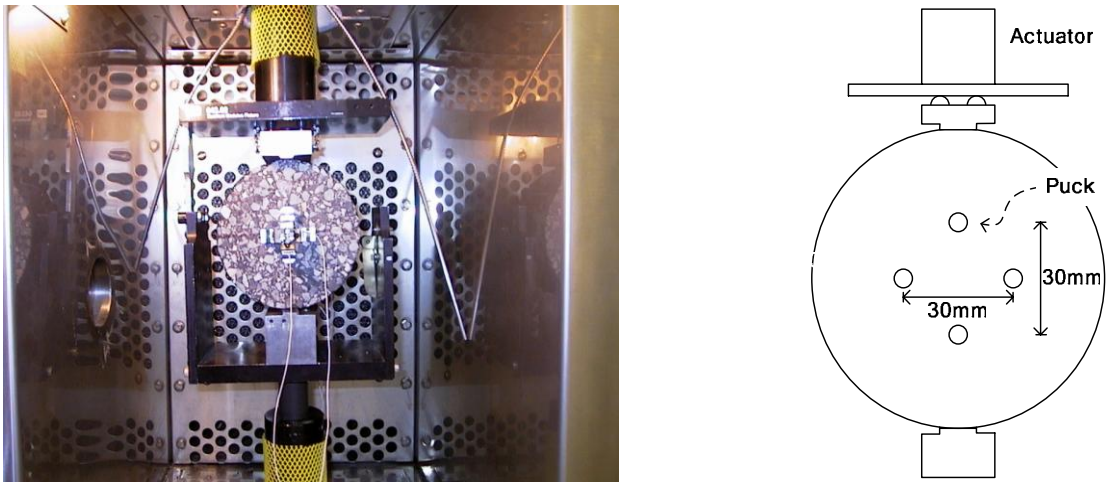

Figure 3.5 Schematic of environment and set up for an IDT

The strains are computed based on the measured deformation and the creep compliance [*D(t)*] using Equation (33) (Kim et al., 2002). Values of the coefficients *c* and *d* in Equation (33) for different specimen sizes are presented in Table 3.6. The gauge length used in this study was

30mm. The corresponding values of *c* and *e* were calculated using the Matlab software and the formula proposed by Kim et al. (2002).

$$D(t) = -\frac{d}{P}\left[cU(t) + eV(t)\right] \tag{33}$$

where

d = the thickness of the test specimen (mm),

P = the applied load (psi),

c, *d* = coefficients related to geometry of the specimen,

U(t) = horizontal strain (mm), and

V(t) = vertical strain (mm).

Table 3.6 Coefficients used to calculate the creep compliance (Kim at el., 2002)

Specimen diameter (mm)	**Gauge Length** (mm)	***c***	***e***
100	27.4	0.7874	2.2783
	30.0	**0.6599**	**1.8710**
	50.8	0.4032	1.024
150	27.4	1.199	3.533
	30.0	**0.9874**	**2.8821**
	50.8	0.611	1.685
	76.2	0.415	1.034

3.4. Test Results

In accordance with the sample preparation, testing procedures, and data analysis described previous section, raw creep compliance values measured in the two testing setups for each mix are represented in Figure 3.6 through Figure 3.9. The test results showed that IDT creep compliances were likely to be more unstable on the whole than uniaxial ones. In addition, there was little change in uniaxial creep compliances at -15°C. This indicates that the compliances may be considered as a glassy compliance of the mixture tested. That is, a material behaves

elastically at the temperature. On the other hand, the IDT creep compliances at -15°C are still changing over time tested. This is because tensile strains exist in the IDT setup creep test. Tensile strain is prone to occur although the applied loading magnitude is relatively low and Equation (33) considers both vertical and tensile strains. In the uniaxial setup, however, only vertical strain occurs when a loading is applied and only the vertical strain is considered when compliances are computed.

Moreover, the results show that there was a significant region of overlap between adjacent temperatures from 20 to 40°C except for the IDT creep test for BM25.0. In contrast, there was a relatively considerable gap between -15 and 20°C, even if the creep curves had still an overlapped region. To construct a reliable CCMC, a sufficiently overlapped region between adjacent creep compliance curves is necessary. However, more reliable CCMC could be constructed if the overlapped regions between adjacent temperatures are similar.

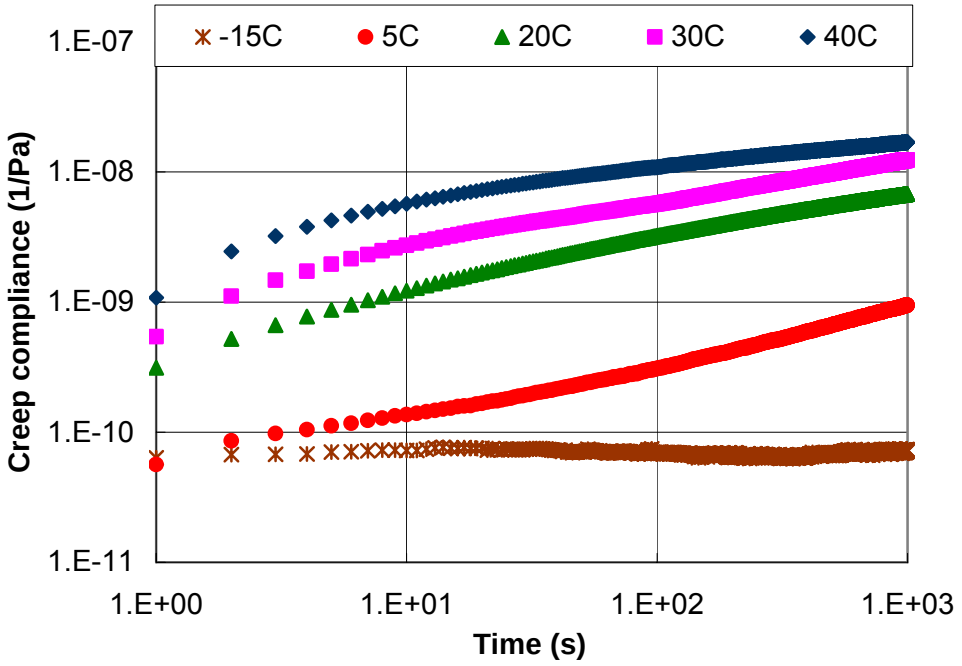

Figure 3.6 Uniaxial creep compliances for the BM25.0

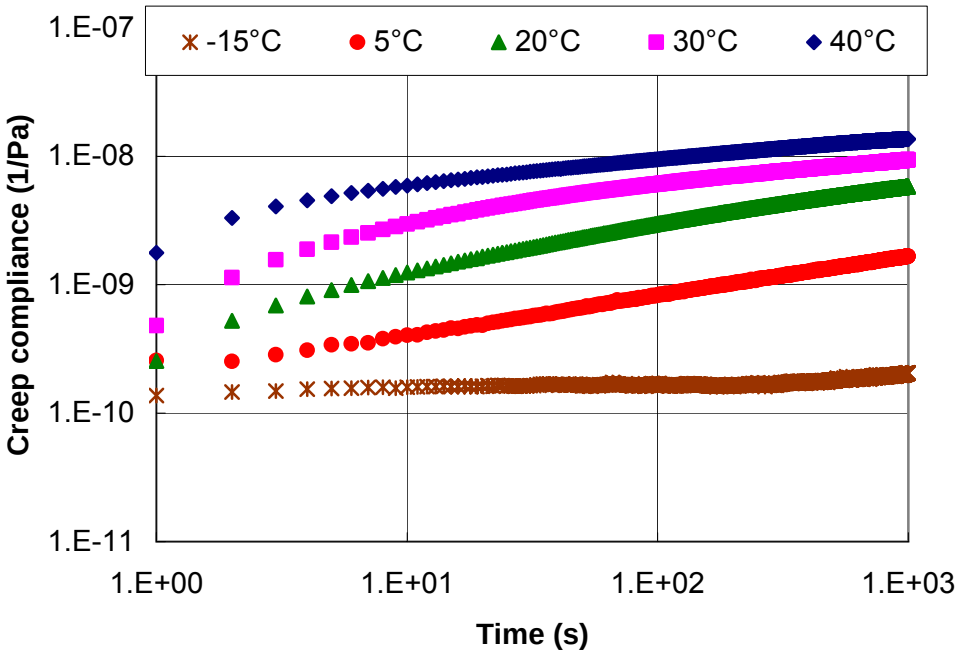

Figure 3.7 Uniaxial creep compliances for the SM9.5A

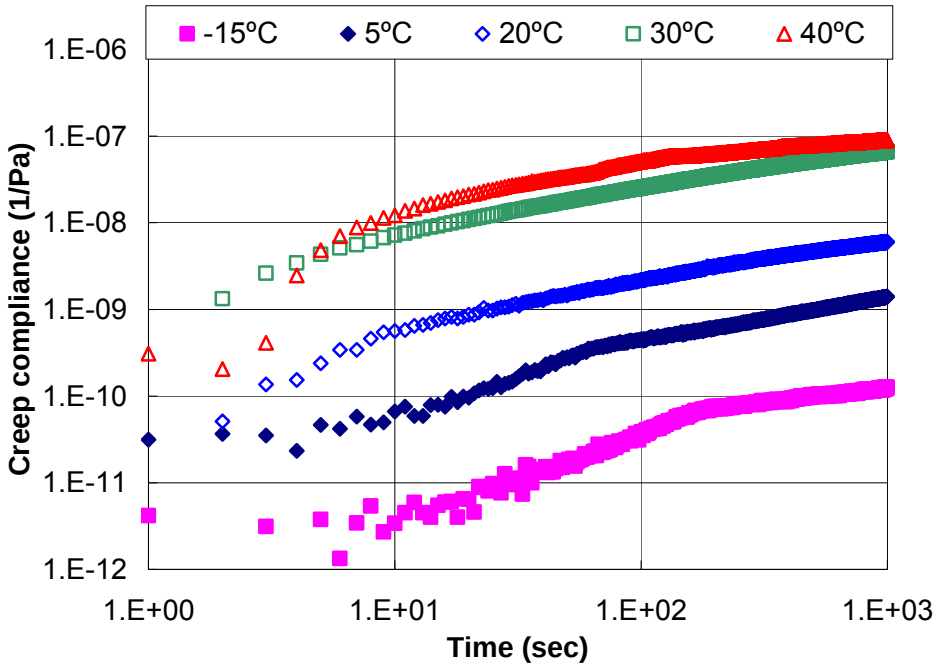

Figure 3.8 IDT creep compliances for the BM25.0

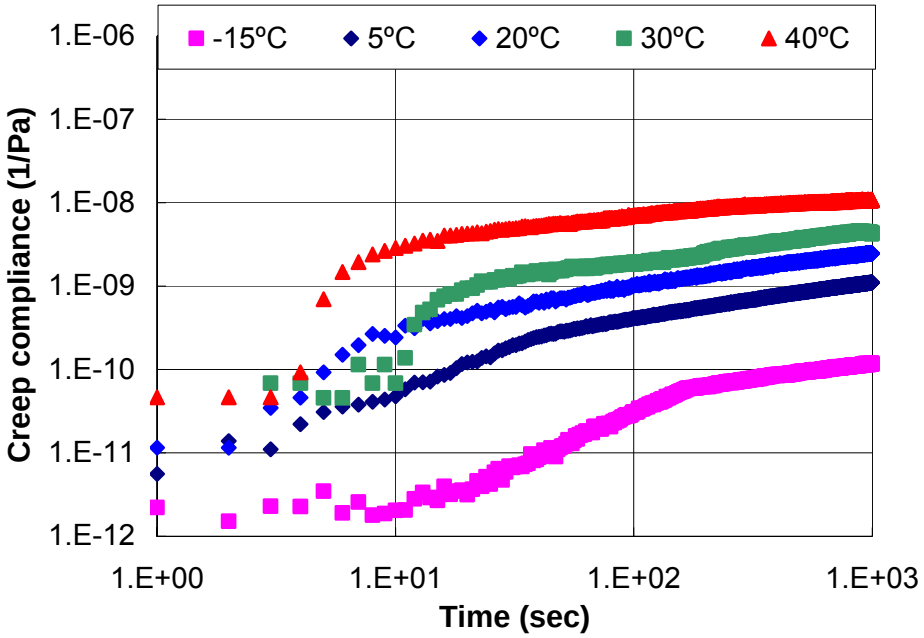

Figure 3.9 IDT creep compliances for the SM9.5A

Chapter 4 Creep Compliance Master Curves

4.1. Introduction

This chapter presents the analysis of the creep compliance tests conducted using the uniaxial and IDT setups. The tests were conducted at five different temperatures: -15, 5, 20, 30, and 40°C. After obtaining individual creep compliance values for 1000 sec at each temperature, the curves were shifted to a reference temperature of 20°C to produce one single smooth curve, the creep compliance master curve (CCMC). Several models were then fitted to the data and the slope of the power model in the logarithmic scale (*m*-value) was used to compare the susceptibility of the mixes to thermal cracking.

4.2. Fitting Creep Compliance Master Curve Models

This section discusses the shifting of the individual creep compliance curves to construct the CCMC and the various mathematical functions used to model the resulting data. Three mathematical functions were investigated: the Prony series, sigmoidal, and power functions.

4.2.1. CCMC Construction

A convenient way to determine the shift factors is to visually shift the creep curve at various temperatures to produce a “smooth” CCMC. This hand shifting method might be arguable because it would appear to cause considerable errors in constructing CCMC. However, Witczak et al. (2000) compared shift factors determined manually with those determined by a computer program (MASTER). The software was developed for the automation of the construction of CCMC as part of NCHRP 9-19 project. The comparison showed that there is little difference between the automatic and manual procedures if the manual shifting is conducted with the aid of a computerized spreadsheet (e.g., EXCEL). The spreadsheet facilitates the trial-and-error process by showing the fit graphically.

An EXCEL spreadsheet was used in this study to find shift factors visually. The different curves were “dragged” in the screen to find the best visual alignment and the shift factor adjusted automatically using the “Goal Seek” function. This function can find the value of a variable that can result in a specific value for a known formula. Table 4.1 presents the resulting shift factors at various temperatures (-15, 5, 20, 30, and 40°C). Figure 4.1 shows that in all cases the trend is approximately linear.

Table 4.1 Summary of creep compliance shift factors

Temperature	Uniaxial		IDT	
	BM	SM	BM	SM
-15°C	4.975	4.559	3.429	3.052
5°C	2.202	2.044	1.251	0.744
20°C	0	0	0	0
30°C	-0.859	-1.042	-1.927	-0.709
40°C	-1.748	-1.978	-2.574	-2.230

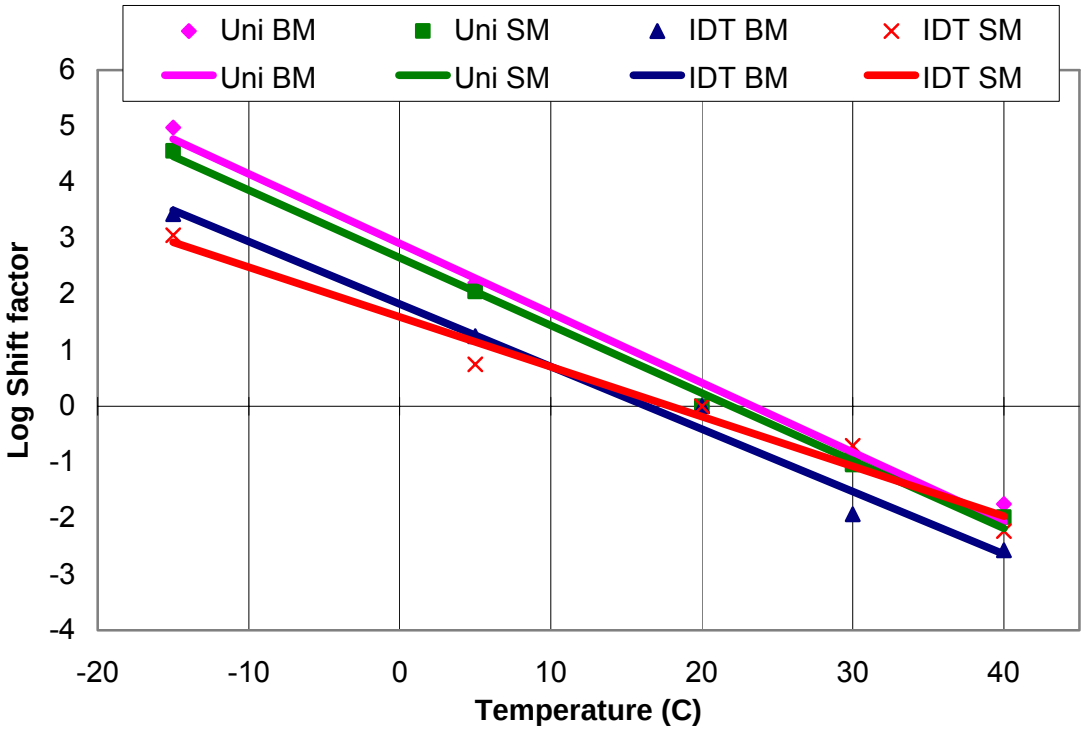

Figure 4.1 Relationship between shift factor and testing temperatures

Figure 4.2 shows the constructed CCMC. The units used are GPa^{-1} because the raw compliance data (in Pa^{-1}) were very close to zero. Noisy creep compliance data measured at the beginning and ending of the creep tests were eliminated from the analysis.

The CCMC constructed for the two different testing setups confirm the finding of Christensen and Bonaquist (2004) that the creep compliance is affected by the testing setup. The plots also suggest that the two mixes evaluated have different CCMC. At low temperatures the uniaxial compliances were higher that those measured using the IDT setup. This can be partially explained because the uniaxial setup measures the creep in pure compression, while that in IDT setup measured is mostly in tension. The relationship at higher temperatures is more complex and it appears to be mix-dependent.

It must be noted that the creep data collected at low temperatures was very noisy, especially while using the IDT setup. This may be partially due to the complex state of stress developed while loading the specimen using this setup. Another reason could be that the measured deformations are so small that they are close to the sensitivity of the extensometers used in the MTS machine. The complicated geometry of the IDT setup also affects the calculation of the creep compliance (e.g., bulging).

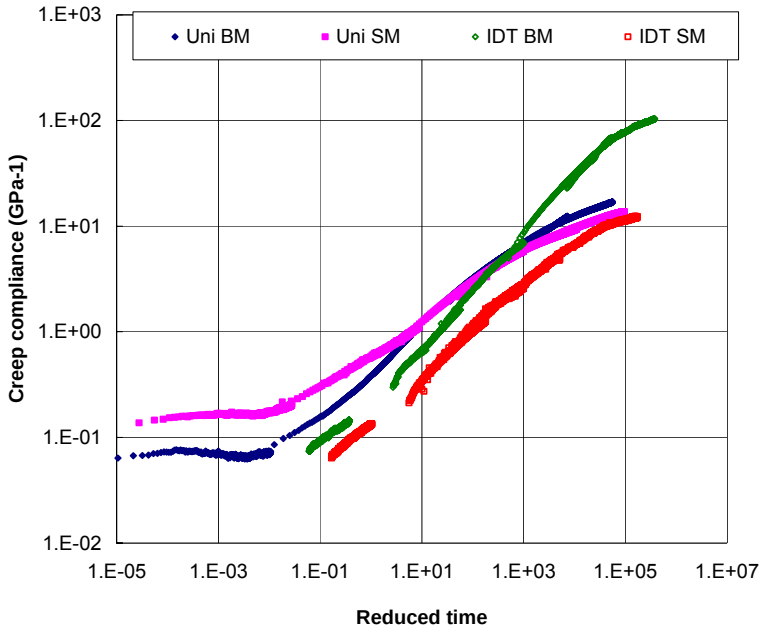

Figure 4.2 CCMCs of each mix and testing setup

4.2.2. CCMC Mathematical Model Fitting

The Prony Series Model

One of the methods used to represent viscoelastic properties is to use decaying exponential representation, commonly called “Prony” or “Dirichlet” series (Park and Kim 2001). As previously described, the Prony series is based on the Maxwell model. The Prony series increases its prediction capabilities as the number of terms is increased. However, at some point the higher order coefficient stops being statistically significant.

Figure 4.3 shows the Prony series fit with one to five terms for a BM25.0 uniaxial CCMC. The coefficients were determined using the SAS software package. It must be noted that the least-square fit was done on an arithmetic scale and for that reason the fit at low reduced times (very small creep compliances) is very poor for the models with lower numbers of terms. A six-term Prony series was also tried but the additional coefficients were not statistically significant. Thus, a five-term model [Equation (34)] was selected.

$$D(t_r) = D_g + \sum_{i=1}^{5} D_i (1 - e^{-t_r/\tau_i}) \tag{34}$$

Table 4.2 summarizes the non-linear regression results for the Prony series model. The statistical Prony series models are compared with the shifted CCMC data in Figure 4.4 and Figure 4.5, for the BM25.0 and SM9.5A mixes, respectively. As expected, in general the models follow the measured data closely.

The Prony series model for the uniaxial CCMC follows the experimental data closely, although the fitted Prony series curves are a little wavy in the logarithmic scale. On the other hand, the differences between the statistical predictions and experimental IDT CCMC are higher at low temperatures. This could be explained by the measurement and data analysis limitations presented earlier in the section.

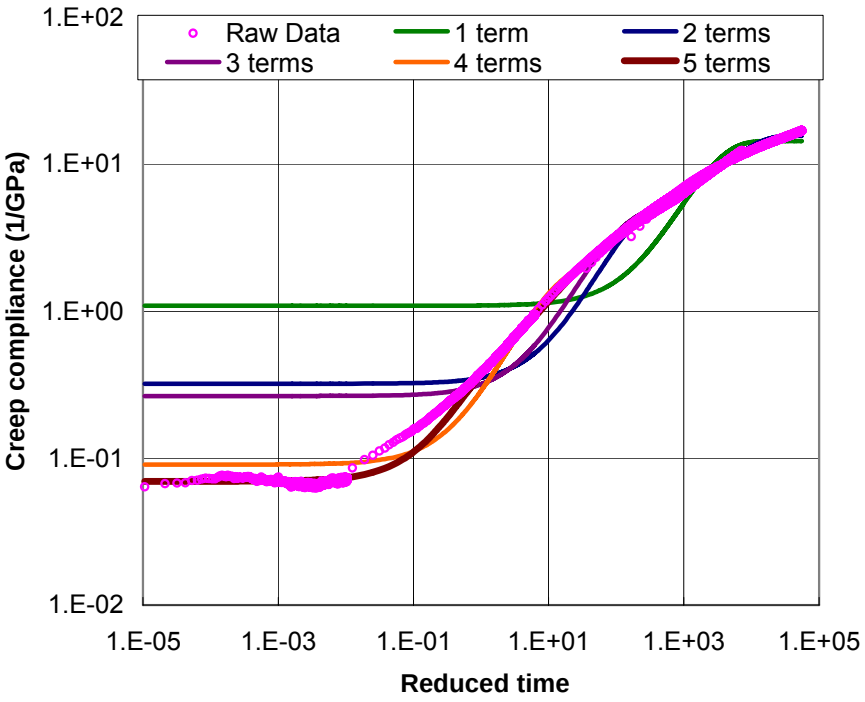

Figure 4.3 The Prony series fit with increasing the number of terms

Table 4.2 Regression results: the Prony series fitting

		Uniaxial		IDT	
		BM	**SM**	**BM**	**SM**
F Value		1052231	3223141	2007677	1347524
Pr>F		<0.0001	<0.0001	<0.0001	<0.0001
R-Square		0.9995	0.9998	0.9998	0.9996
Least-square Estimate for the Prony Series Coefficients	D_g	0.0695	0.1779	0.0719	0.0846
	D_1	0.3534	0.5667	0.2184	0.2835
	τ_1	1.0739	1.1788	1.148	9.1336
	D_2	1.32	2.2899	2.0212	1.0769
	τ_2	17.6127	62.7561	69.7343	167.1
	D_3	2.8247	3.3976	44.5864	6.048
	τ_3	184.1	779.3	28522.1	16307.7
	D_4	6.9871	3.3472	13.6771	2.071
	τ_4	3100.9	9977.3	3235.2	1501.4
	D_5	8.2219	4.7423	50.4167	4.0234
	τ_5	52695.4	55521.0	202826	159088

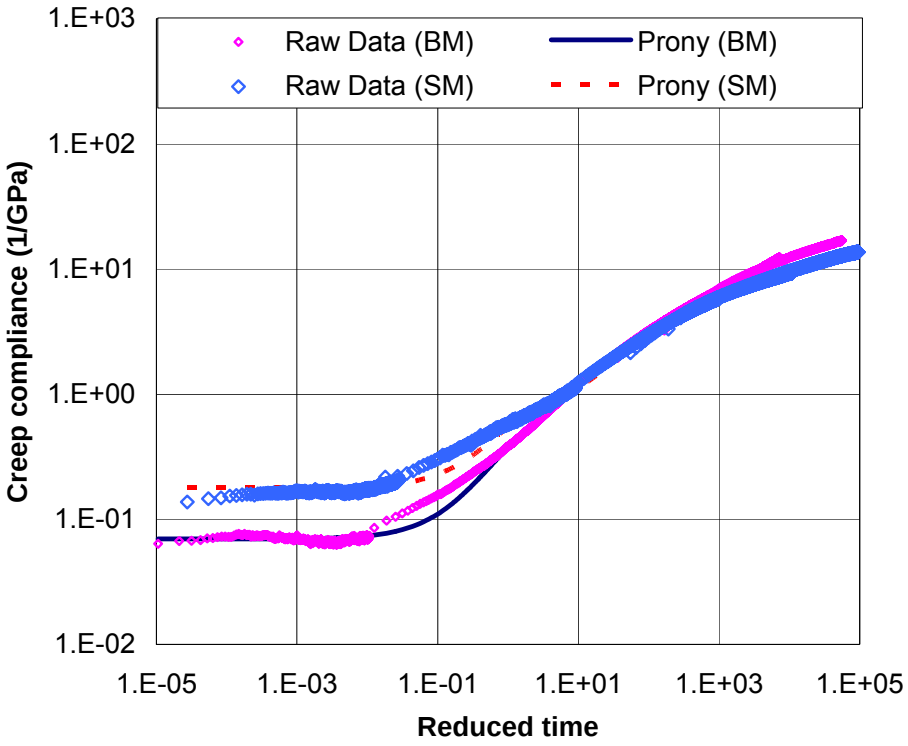

Figure 4.4 Prony series models for the uniaxial CCMC

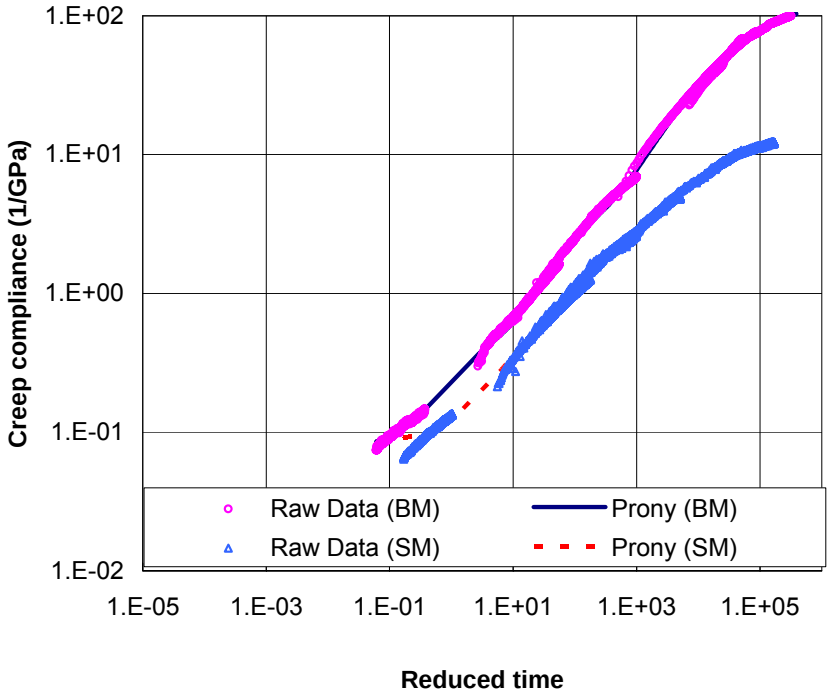

Figure 4.5 Prony series models for the IDT CCMC

The Sigmoidal Model

Pellinen and Witczak (2002) proposed a sigmoidal function for modeling the dynamic modulus master curve. In this investigation the sigmoidal model was also used for fitting the CCMC data obtained from both testing setups. The sigmoidal function is presented in Equation (35):

$$\log\left|D(t_r)\right| = \delta - \frac{\alpha}{1+e^{\beta+\gamma\log t_r}} \tag{35}$$

Coefficients of the model have meaningful physical significance (Figure 4.6). For instance, the coefficients of β and γ determine the shape of the sigmoidal function model. A sigmoidal functional curve will move to the left and become stiffer with the increase of β and γ, respectively. The coefficient $\delta-\alpha$ and δ represent the minimum and maximum values of the creep compliance, respectively. The coefficient $\delta-\alpha$ represents the equilibrium (glassy) compliance at very small times [$D_g = \lim_{t\to 0} D(t)$].

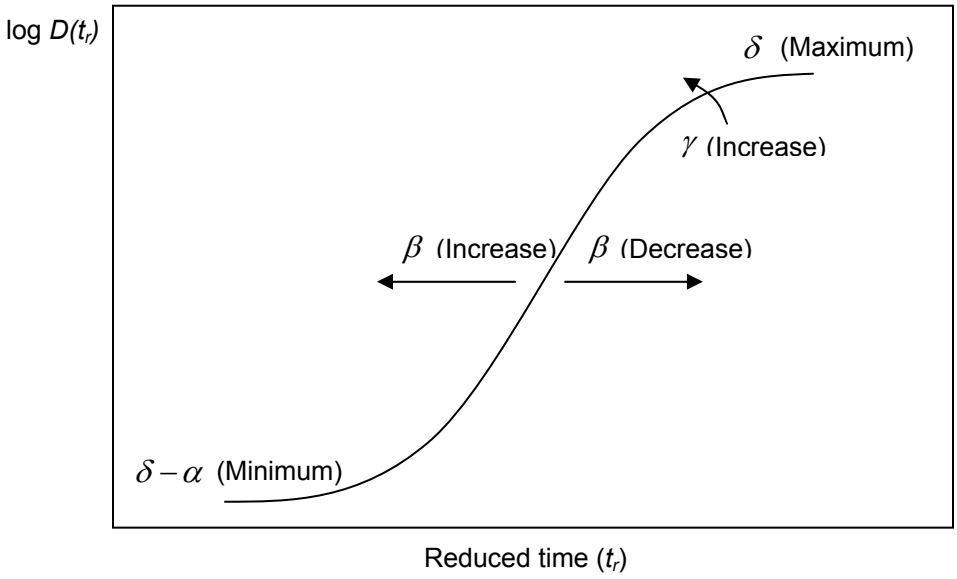

Figure 4.6 Effect of the sigmoidal function coefficients on the CCMC

(After Pellinen and Witczak, 2002)

The best-fit sigmoidal functions for each CCMC were determined using the SAS statistical package. Table 4.3 summarizes the regression analysis results. As expected, the model fitted the curves well, especially at high temperatures (Figure 4.7 and Figure 4.8).

Table 4.3 Regression results: Sigmoidal function fitting

		Uniaxial		IDT	
		BM	SM	BM	SM
F Value		1170581	2181328	1497821	2510806
Pr>F		<0.0001	<0.0001	<0.0001	<0.0001
R-Square		0.9986	0.9992	0.9998	0.9996
Parameter Coefficient	δ	1.4138	1.2825	2.7379	1.4459
	α	2.8726	2.2737	4.4302	3.2149
	β	-0.5693	-0.7796	-1.2069	-0.9598
	γ	0.6602	0.6694	0.5275	0.5907

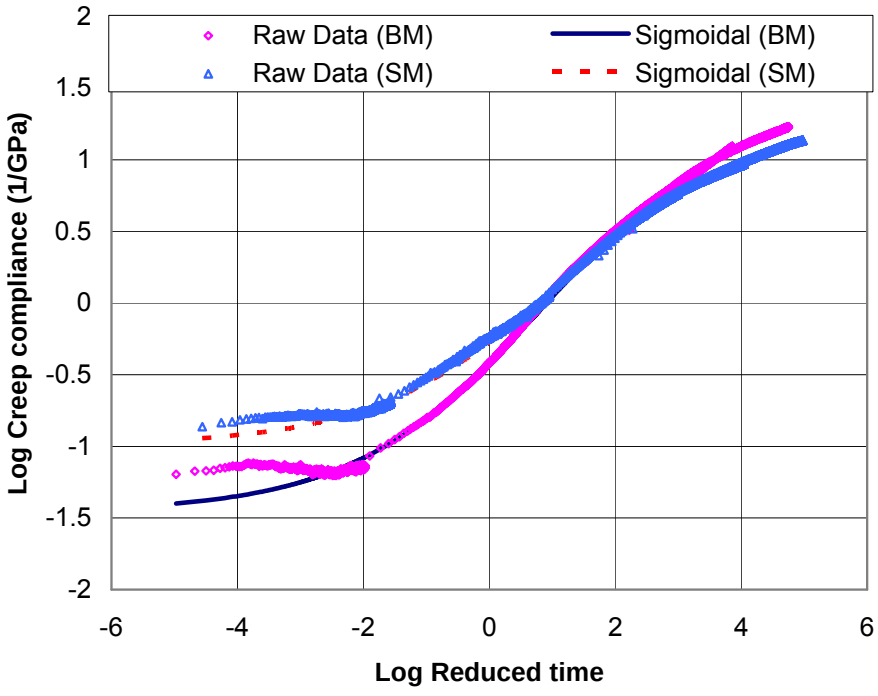

Figure 4.7 Sigmoidal models for the uniaxial CCMC

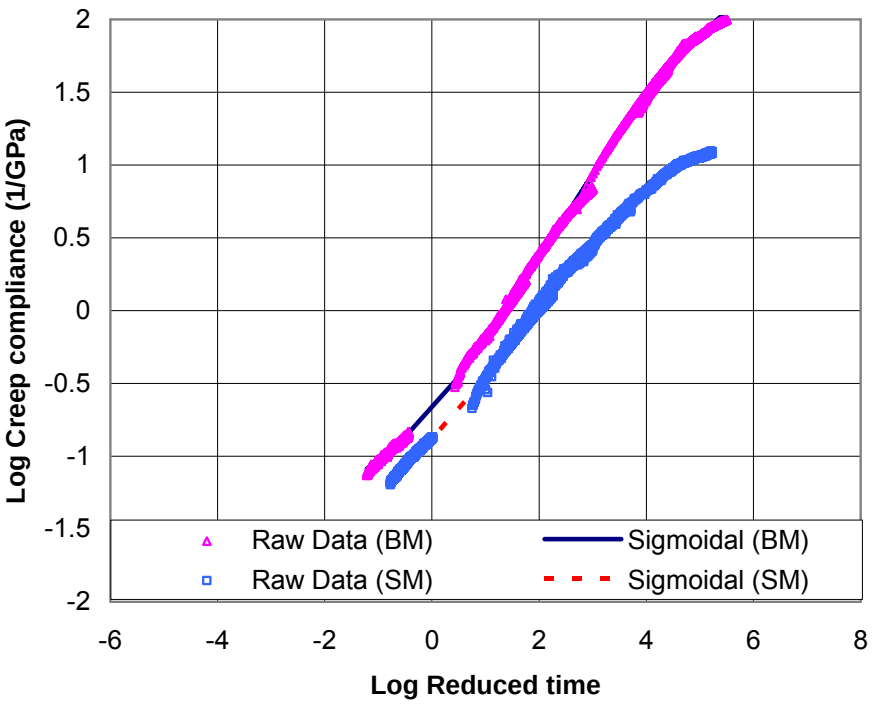

Figure 4.8 Sigmoidal models for the IDT CCMC

The Power Model

The power model has been widely used to represent the linear part (on a logarithmic scale) of the CCMC. The primary reason to use this power form [Equation (36)] is to find the *m*-value, which is essentially the slope of the CCMC on a logarithmic scale.

$$D(t_r) = D_0 + D_1 t_r^{\ m} \tag{36}$$

Even if the power model is unable to account for CCMC at long times, the *m*-value is considered an important parameter because it is used to predict thermal distress at low temperatures. For this reason, two sets of power models were determined. The first set was obtained using the entire CCMC (Figure 4.9 and Figure 4.10). The purpose was to compare the fitting with the previous models. For the second set, fitting was performed using only the lower temperatures. The best-fit models were again obtained from regression analysis using the SAS package. Table 4.4 summarizes the regression analysis results.

Table 4.4 Regression results: Power function fitting

		Uniaxial		IDT	
		BM	SM	BM	SM
F Value		561593	672038	1123080	1021009
Pr>F		<0.0001	<0.0001	<0.0001	<0.0001
R-Square		0.9986	0.9992	0.9998	0.9996
Parameter Coefficient	D_0	0.0246	0.0656	0	0
	D_1	0.3951	0.5024	0.3022	0.176
	m-value	0.4497	0.3681	0.4953	0.399

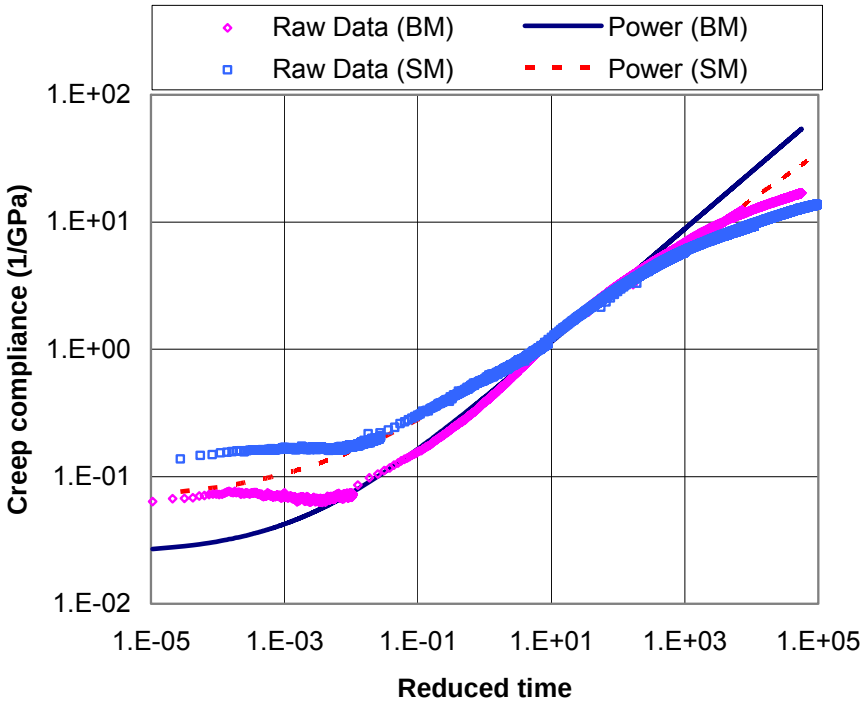

Figure 4.9 Power models for the uniaxial CCMC

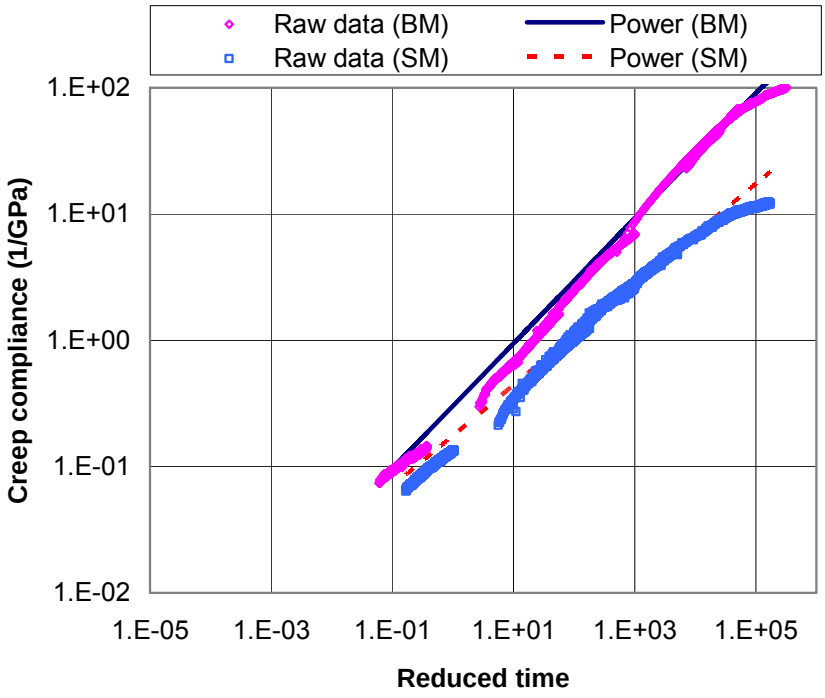

Figure 4.10 Power models for the IDT CCMC

4.3. Effect of the Thermal Cracking Model using the *m*-value

As previously discussed, the slope of CCMC, the *m*-value, is used to determine the change of thermal cracking rate on pavement surface at low temperatures. Since the power models fitted in the previous section did not work very well at low temperatures, a new regression model was derived using only the data obtained at -15 and 5°C (Figure 4.11 and Figure 4.12). The resulting parameter coefficients and other statistical information are summarized in Table 4.5.

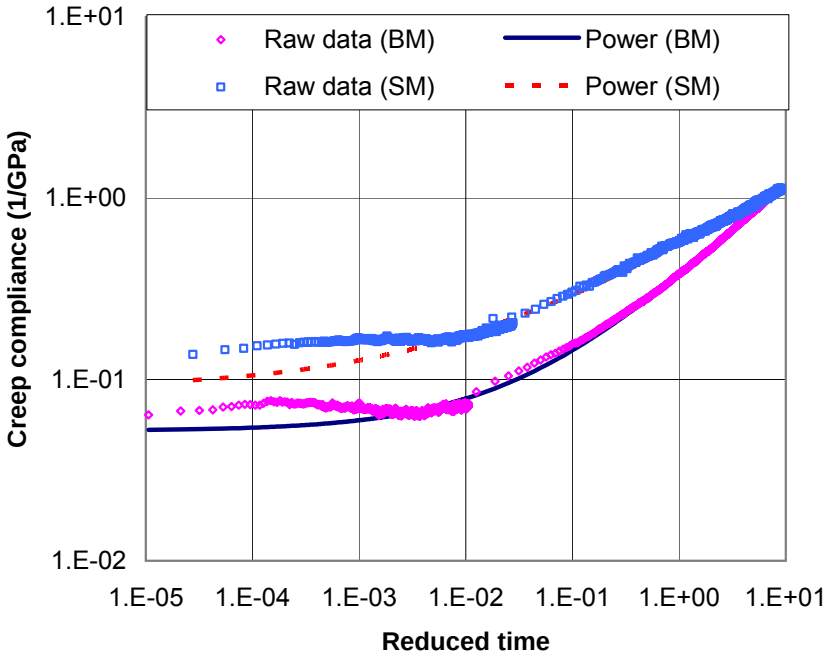

Figure 4.11 The power model at low temperatures from uniaxial setup

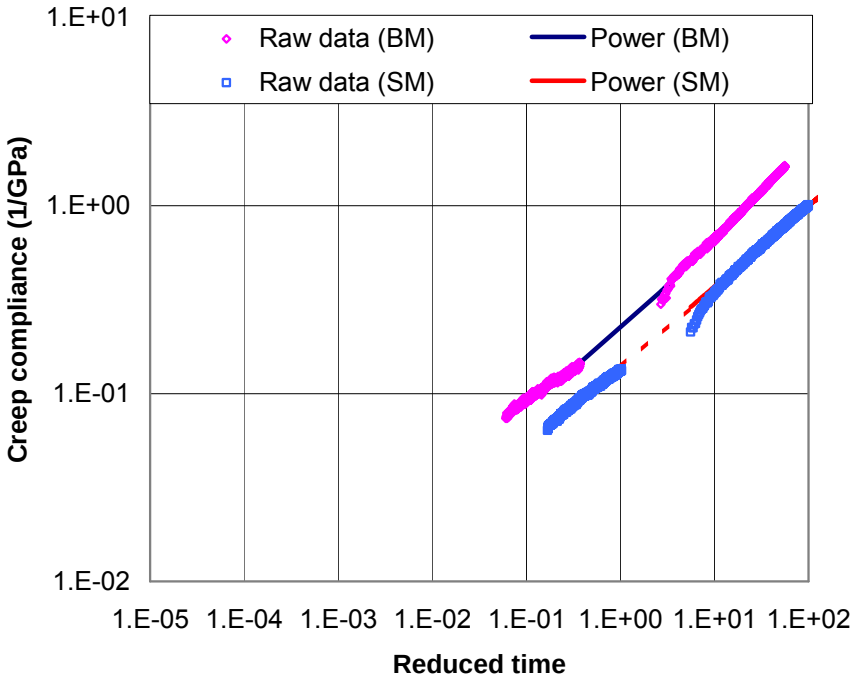

Figure 4.12 The power model at low temperatures from IDT setup

Table 4.5 Regression results: Power model at low temperatures

		Uniaxial		IDT	
		BM	**SM**	**BM**	**SM**
F Value		3740233	712888	4329972	378739
Pr>F		<0.0001	<0.0001	<0.0001	<0.0001
R-Square		0.9997	0.9986	0.9998	0.9995
Parameter Coefficient	D_0	0.0521	0.0883	0.0374	0
	D_1	0.3272	0.4680	0.1840	0.1382
	m-value	**0.5479**	**0.3599**	**0.5344**	**0.4293**

The determined *m*-values for each mix and testing type are presented in Figure 4.13. The results show that BM25.0 has higher *m*-value than SM9.5A regardless of the testing setups. The relationship between the *m*-value and thermal cracking susceptibility could be explained if a typical *K*-value were found. However, investigating K-value is out of scope of this research so it could not be concluded to investigate the effect of thermal cracking using the m-values. This is left for a future research.

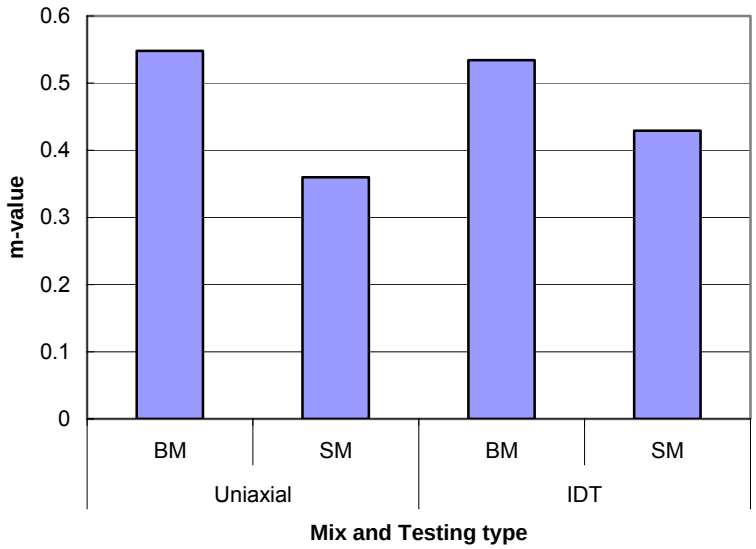

Figure 4.13 *M*-values for both mixes obtained from the power models

4.4. Summary

Creep compliance data of different asphalt mixtures were determined from creep test at five temperatures (-15, 5, 20, 30, and 40°C) with different testing setups: uniaxial compressive and indirect tension. Using the time-temperature superposition principle, the creep compliance curve at each temperature was shifted to a reference temperature (20°C) to make a single smooth line: the creep compliance master curve (CCMC). Shifting factors for each asphalt mixture were visually determined with the aid of the Goal Seek function of the EXCEL spreadsheet.

Three mathematical models (the Prony series, sigmoidal, and power) were fitted to the CCMC data using regression analysis. The result indicated that the sigmoidal model was the one that best fit the data over the entire range of reduced times considered.

The susceptibility of mixes to thermal cracking was investigated using the *m*-value determined at low temperatures. The BM25.0 has higher *m*-values than SM9.5A; however, a decision regarding which mix is more susceptible to thermal cracking at low temperatures using *m*-value could not be made.

Chapter 5 Interconversion between the Dynamic Modulus and Creep Compliance

5.1. Introduction

This chapter presents the results of the interconversion between the various viscoelastic properties measured: the dynamic modulus, creep compliance and relaxation modulus. Two sets of conversions were performed. The first one was to convert the dynamic modulus into creep compliance. Approximate methods were used to convert the dynamic modulus to relaxation modulus, and then the relaxation modulus to creep compliance. The predicted creep compliance was compared with the creep compliance that was experimentally obtained in the lab. The second conversion consisted of predicting the dynamic modulus from lab-determined creep compliance. An exact method was used in this case for converting the creep compliance to complex compliance and then to dynamic modulus. The predicted dynamic modulus was again compared with the dynamic modulus measured in the lab.

5.2. Conversion from the Dynamic Modulus to Creep Compliance

5.2.1. Prediction of the Relaxation Modulus from the Dynamic Modulus

The first step consisted of predicting the relaxation modulus from the dynamic modulus of asphalt mixtures using the interconversion method described in Equation (28). The dynamic modulus and phase angle were measured using a uniaxial testing setup at five different temperatures (Flintsch et al., 2005). The storage modulus (*E'*) was calculated using the dynamic modulus and phase angle [Equation (14)] and then plotted on logarithmic scale. A sigmoidal function was fitted to the storage modulus data using a curve-fitting software (CurveExpert 1.3). The measured and predicted storage moduli are presented in Figure 5.1 to Figure 5.3. Using the regressed analytical function, the local logarithmic slope of the storage modulus (*n*) was then computed over the specified frequency range using Equation (20). The function *n* is the derivative of the log of $E'(\omega_r)$ with respect to the log of ω_r, at a particular time. The predicted relaxation moduli were then computed and plotted in Figure 5.2 and Figure 5.4.

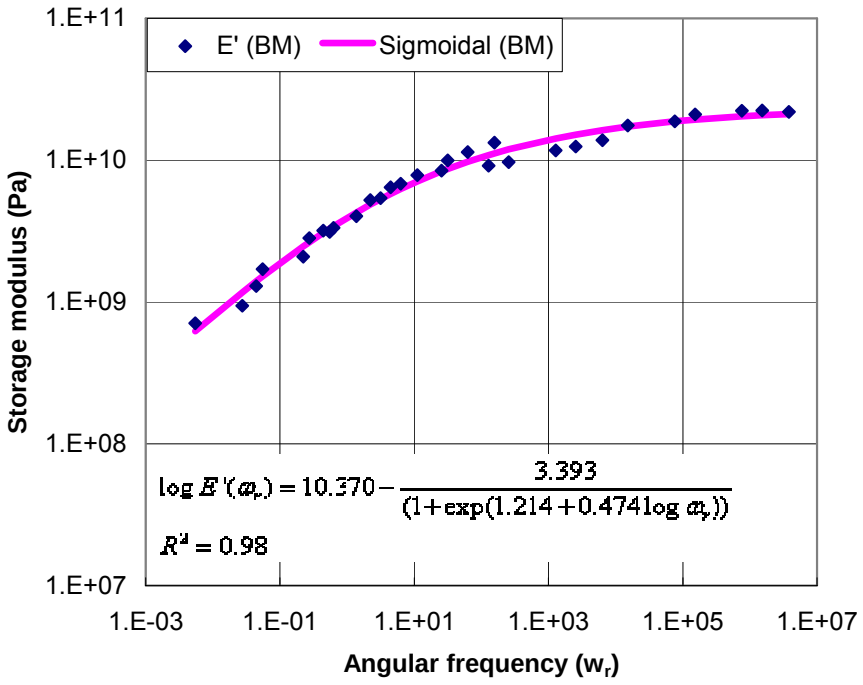

Figure 5.1 Storage modulus and sigmoidal fitting curve (BM25.0)

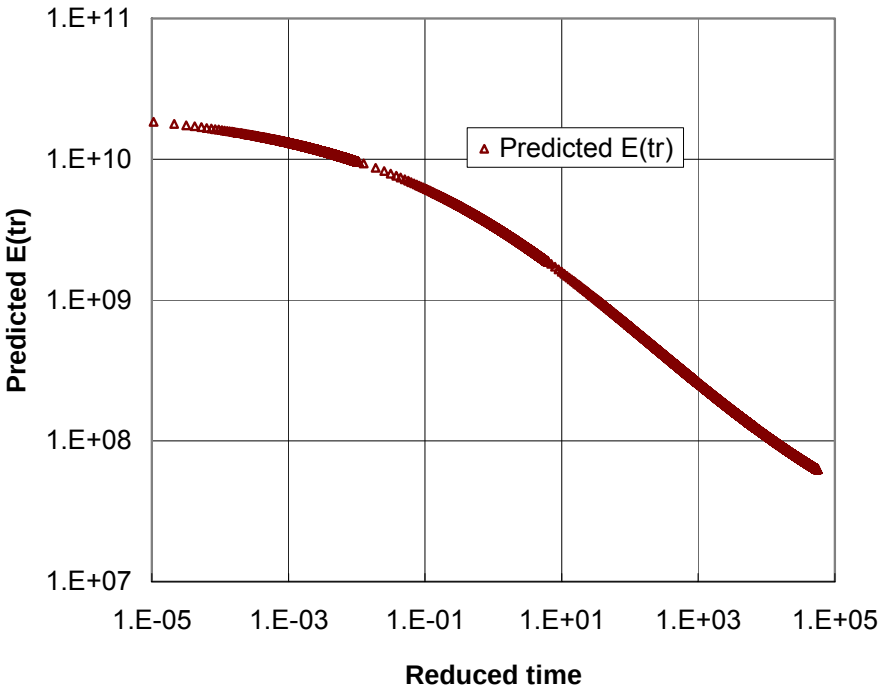

Figure 5.2 Predicted relaxation modulus (BM25.0)

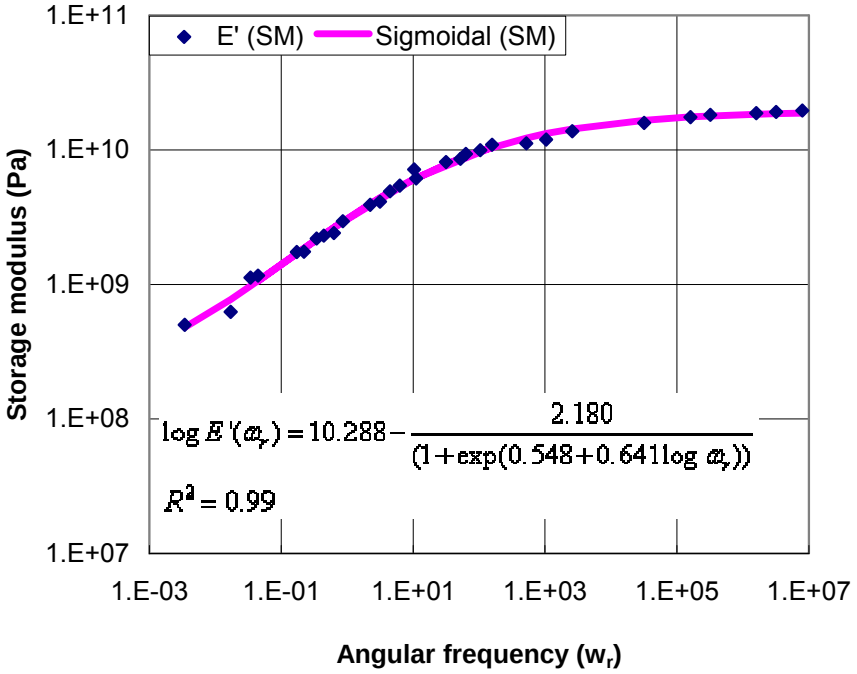

Figure 5.3 Storage modulus and sigmoidal fitting curve (SM9.5A)

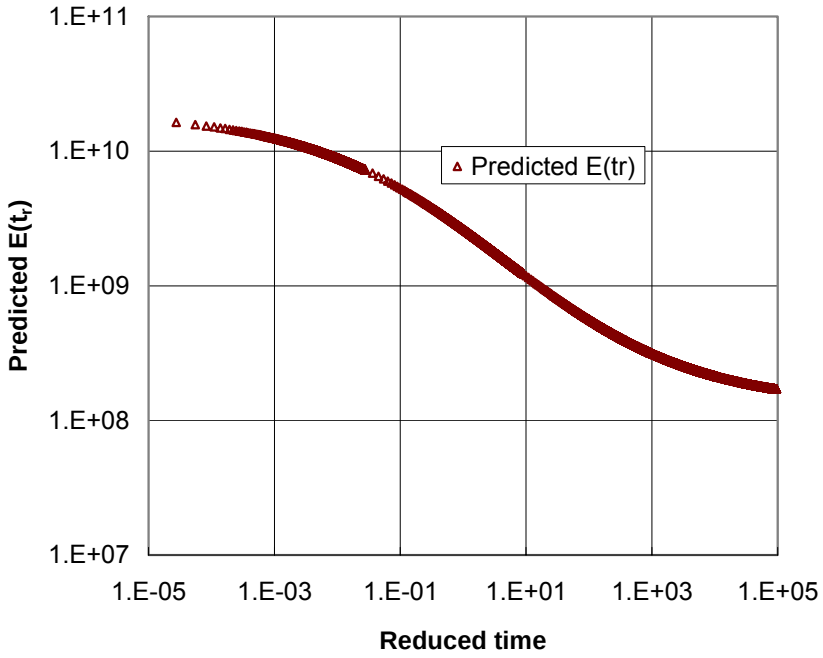

Figure 5.4 Predicted relaxation modulus (SM9.5A)

5.2.2. Prediction of the Creep Compliance from the Relaxation Modulus

The second step for converting the dynamic modulus into the creep compliance consisted in predicting the creep compliance from the relaxation modulus obtained in the previous section using the approximate interconversion method [Equation (19)]. The local logarithmic slopes at each reduced time point was determined and used to compute the relaxation modulus. The relaxation modulus data was then fitted with a sigmoidal function; and the models in Equations (37) and (38) were obtained for the BM25.0 and SM9.5A, respectively:

$$\log E(t_r) = 10.279 - \frac{2.172}{(1+\exp(0.429 - 0.647\log t_r))} \quad (37)$$

$$\log E(t_r) = 10.368 - \frac{3.409}{(1+\exp(1.126 - 0.473\log t_r))} \quad (38)$$

The values of their local derivatives over reduced time ranges were used in Equation (20) to evaluate the creep compliance. The converted creep compliance master curves (CCMC) for BM25.0 and SM9.5A are shown in Figure 5.5 and Figure 5.6.

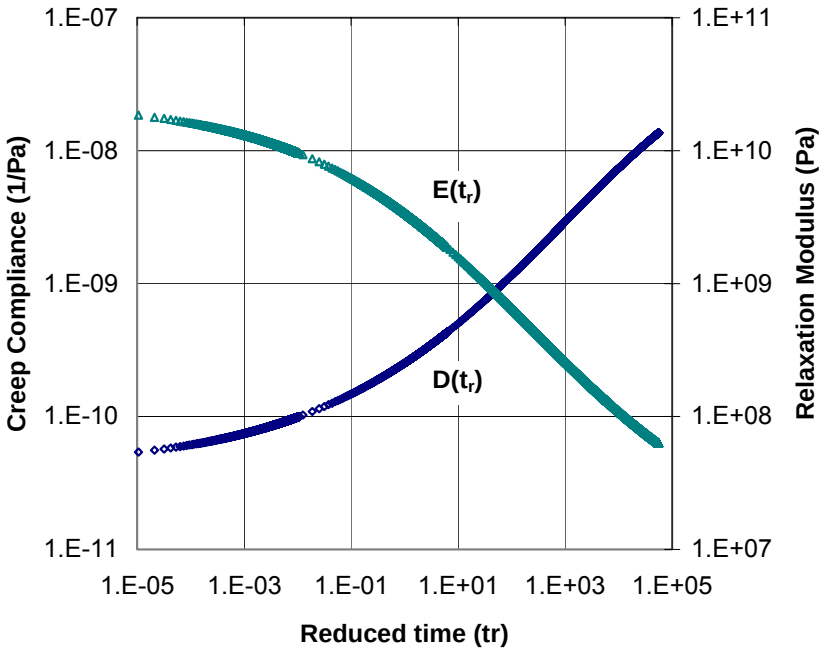

Figure 5.5 The relaxation modulus and predicted creep compliance (BM25.0)

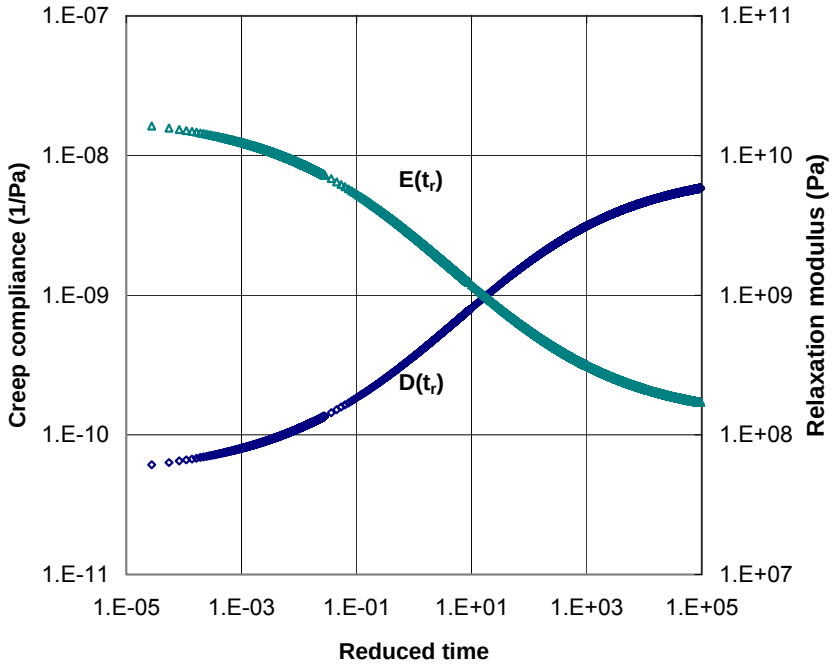

Figure 5.6 The relaxation modulus and predicted creep compliance (SM9.5A)

5.2.3. Comparison of Computed versus Measured Creep Compliances

The lab-determined and predicted creep compliances are compared in Figure 5.7 and Figure 5.8. Although the values are in the same order of magnitude, there is a relatively large discrepancy among the measured and predicted CCMC. The following two reasons are thought to contribute to the differences:

- All the interconversion methods found in the literature assume that the material is linearly viscoelastic to avoid the complexity of nonlinear analysis. Representing viscoelastic properties with spring and dashpot is a good example. However, viscoelastic materials in the real world behave nonlinearly.

- The other potential reason may lie on the variation of specimens used in this study. Although the differences are not very large, each specimen tested had slightly different air void contents and G_{mb}. In addition, the different sample geometries result in different air void distributions within the specimens.

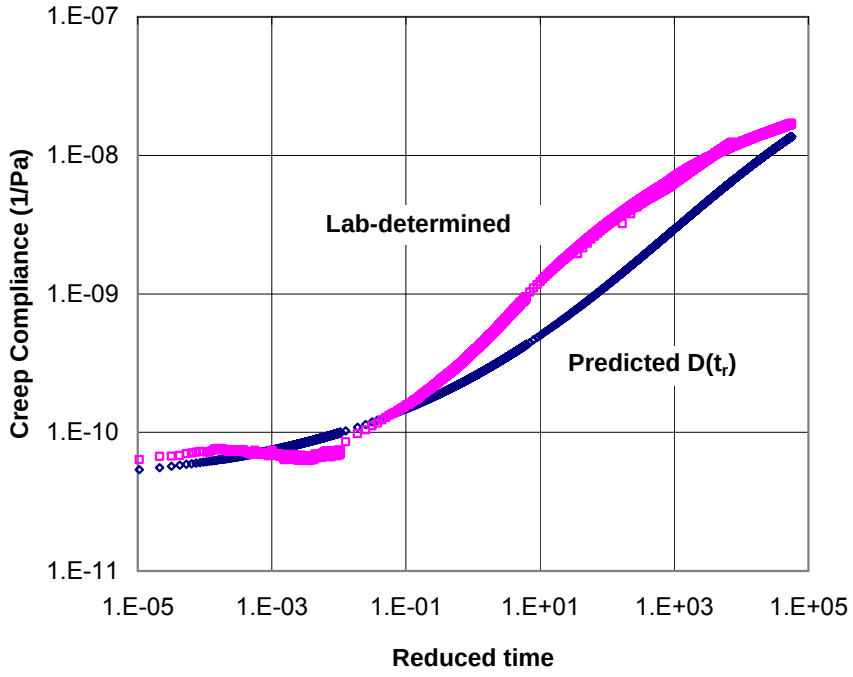

Figure 5.7 Comparison of the creep compliance predicted from the dynamic modulus and determined in the lab test (BM25.0)

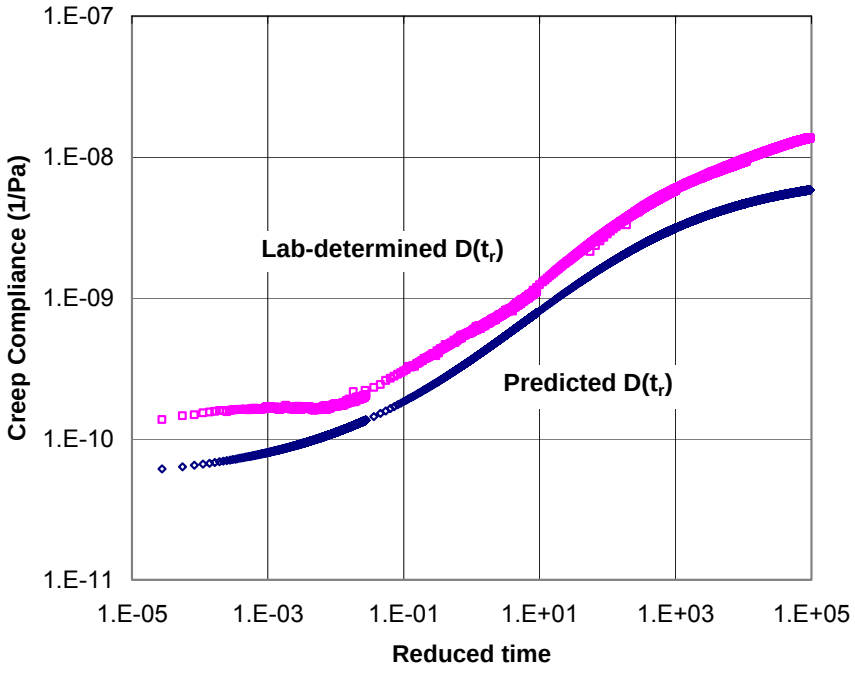

Figure 5.8 Comparison of the creep compliance predicted from the dynamic modulus and determined in the lab test (SM9.5A)

5.3. Comparison from the Creep Compliance to the Dynamic Modulus

Conversion of the creep compliances to dynamic moduli was performed using the exact interconversion method described in Equations (23) through (27). The best-fit CCMC Prony series models for the two mixes [Equations (39) and (40)] were used to describe the creep compliance. The creep compliance was converted into the dynamic modulus and plotted in Figure 5.9 and Figure 5.10.

$$D(t_r) = 0.0695 + 0.3534(1 - e^{-t_r/1.0739}) + 1.32(1 - e^{-t_r/17.6127}) + 2.8247(1 - e^{-t_r/184.1}) + 6.9871(1 - e^{-t_r/3100.9}) + 8.2219(1 - e^{-t_r/52695.4}) \quad (39)$$

$$D(t_r) = 0.1779 + 0.5667(1 - e^{-t_r/1.1788}) + 2.2899(1 - e^{-t_r/62.7561}) + 3.3976(1 - e^{-t_r/779.3}) + 3.3472(1 - e^{-t_r/9977.3}) + 4.7423(1 - e^{-t_r/55521}) \quad (40)$$

The converted dynamic modulus appears wavy in the logarithmic scale because the original analytical form of creep compliance is based on the Prony series. The measured and predicted dynamic moduli are compared in Figure 5.11 and Figure 5.12. As expected, there are some obvious differences but again the values are of the same order of magnitude.

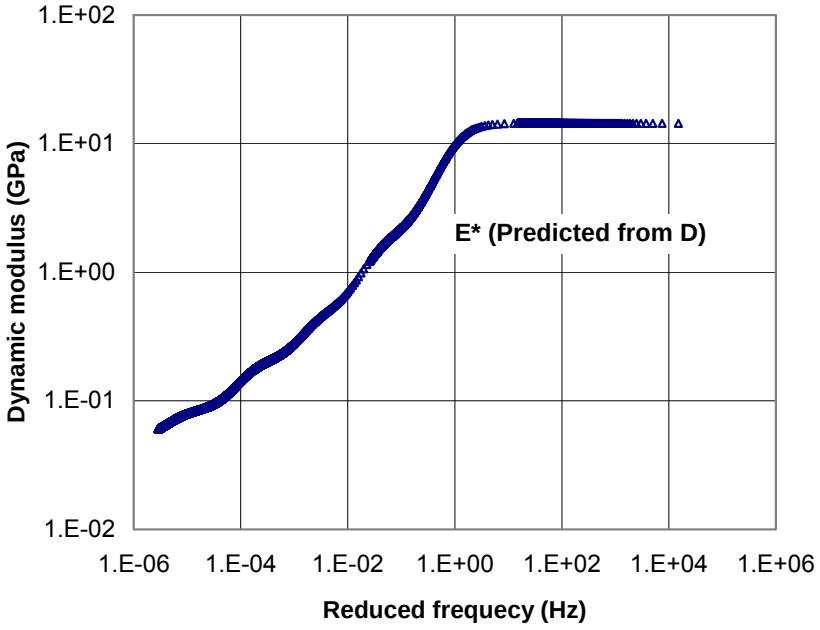

Figure 5.9 The predicted dynamic modulus (BM25.0)

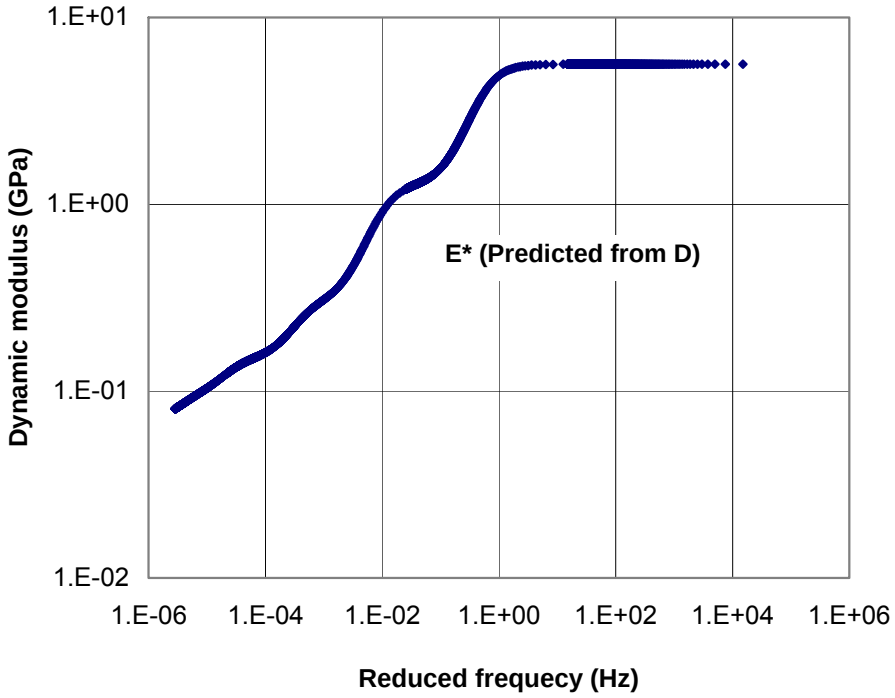

Figure 5.10 The predicted dynamic modulus (SM9.5A)

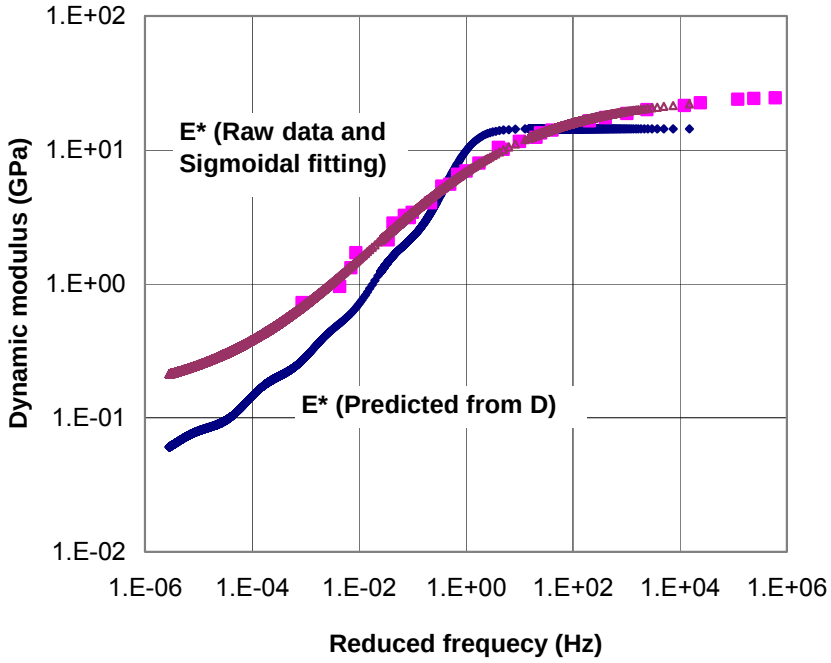

Figure 5.11 Comparison of the predicted and measured dynamic moduli (BM25.0)

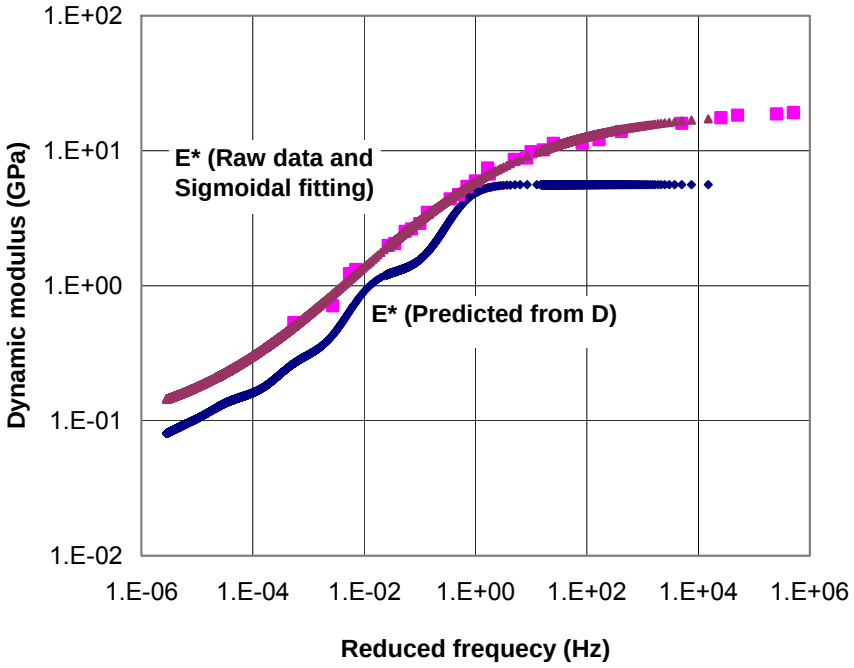

Figure 5.12 Comparison of predicted and measured dynamic moduli (SM9.5A)

5.4. Summary

Conversions among linear viscoelastic properties, namely the dynamic modulus, creep compliance and relaxation modulus, were conducted using approximate and exact methods. The creep compliance determined in the lab was compared with that predicted from the dynamic modulus. Also, the dynamic modulus determined in the lab was compared with that predicted from the creep compliance. The theory of viscoelasticity permits these comparisons because the viscoelastic properties encode the same information regardless of their form. There were noticeable differences between the measured and predicted properties in all cases. These differences are thought to be due actual nonlinearity in the material response when all of the reviewed interconversion methods assume that the viscoelastic materials behave linearly at all times (frequencies) and temperatures.

Chapter 6 Findings, Conclusions, and Recommendations

The creep compliance of two HMA mixes were measured in different testing setups (uniaxial compressive and indirect tensile setups) and at various temperatures. Creep compliance master curves (CCMCs) were constructed using the time-temperature superposition and modeled using three mathematical functions: the Prony series, power, and sigmoidal. The SAS statistical package was used to find the best-fit model for each mix and testing configuration and the obtained models were investigated and compared. Using the *m*-value obtained from the power model, the susceptibility to thermal cracking at low temperatures of the mixes was evaluated. Finally, CCMC obtained from the dynamic modulus test and interconversion procedures were compared with the CCMC determined experimentally using the uniaxial setup.

6.1. Findings

Several findings regarding creep compliance measurement and its application were produced in this research. The main findings are summarized below:

- Creep compliance measurements at low temperatures were noisier than at high temperatures. This was probably because the magnitude of the measurements approaches the sensitivity of the measurement gauges. Furthermore, creep measurements with the IDT setup were noisier, probably because the testing geometry, stress/strain distribution, and method to calculate creep compliance are more complex in this configuration.
- The compliance data determined using the two testing setups were noticeably different. At low temperatures, the uniaxial compressive creep was higher than that measured in the IDT mode. This is consistent with previous findings. At higher temperatures the relationship appears to be mix-dependent.
- To construct a more reliable master curve, the testing temperatures should be adjusted especially between -15 and 5°C. The temperatures chosen for the investigation did not produce enough overlap between the low temperature shifted curves. More overlap between curves obtained at adjacent temperatures would increase the reliability of the master curve.

- The regression analysis conducted to fit the CCMC data indicate that the three mathematical functions considered are appropriate to model the CCMC. The sigmoidal function produced the best fit over the entire range of reduced times investigated for both testing setups.
- Of the various Prony terms investigated, the five-term Prony series proved to be the most appropriate for modeling the experimental CCMC data. However, the fitting was not very good at low temperatures, probably because the least-square fitting was conducted in the arithmetic scale (instead of using a logarithmic transformation).
- The *m*-values for BM25.0 were higher than those for SM9.5A regardless of the testing setup used to measure the creep compliance.
- The dynamic modulus determined in a uniaxial setup was successfully converted into creep compliance with the same setup. However, although they were in the same order of magnitude the predicted and measured values are noticeably different. This is thought to be due to nonlinear behavior of viscoelastic material. The sigmoidal function performed better than the Prony series when used in the interconversion procedure because of the Prony series model was too wavy.

6.2. Conclusions

The results of the experimental program conducted support the conclusion that the three mathematical models considered (the Prony series, power and sigmoidal) are appropriate to model the CCMC over a wide range of reduced times. However, the sigmoidal model produced the best fit over the entire range investigated. This model also produced the best results when used in the interconversion procedures. A noticeable difference was observed between the CCMC predicted from dynamic modulus measurements and those obtained experimentally, this is probably because the interconversion method is based on the assumption that the material displays linear viscoelasticity.

6.3. Recommendations

Based on the results of this study, the following recommendations can be made to improve the development of the CCMC and to obtain a stronger conclusion in future investigations.

- The set of testing temperatures should be revised to produce more overlap between the shifted adjacent curves. This would allow the development of more reliable shifting, and consequently better CCMC. Temperature increments of less than 10°C over the entire range of temperatures are recommended.
- The sigmoidal function should be used to model the CCMC of HMA over a large range of reduced times. The power model produces good results at low temperatures and should continue to be used to assess the susceptibility of HMA to thermal cracking.
- The conversion of the creep compliance into the dynamic modulus and vice versa appears to work better when using a sigmoidal function than when using the Prony series recommended in the literature. The sigmoidal function produces a smoother CCMC. Furthermore, it may be necessary to shift the converted CCMC to account for nonlinearity in the behavior of the HMA. More mixes should be investigated to assess the feasibility of defining correction shift factors.

References

AASHTO T332-03. *Determining the Creep Compliance and Strength of Hot Mix Asphalt (HMA) Using the Indirect Tensile Test Device*. American Association of State Highway and Transportation Officials, 25th edition, 2005.

Brown, E.R. and K.Y. Foo, "Comparison of Unconfined- and Confined-Creep Tests for Hot Mix Asphalt," *Journal of Materials in Civil Engineering,* Vol. 6, No. 2, pp. 307-326, May, 1994.

Buttlar, W.G. and R. Roque, "Development and Evaluation of the Strategic Highway Research Program Measurement and Analysis System for Indirect Testing at Low Temperatures," *Transportation Research Record No.1454*, Transportation Research Board, Washington, D.C., pp. 163-171, 1994.

Christensen, D.W. and R.F. Bonaquist, "Evaluation of Indirect Tensile Test (IDT) Procedures for Low-Temperature Performance of Hot Mix Asphalt," NCHRP Report 530, Transportation Research Board, Washington DC, 2004.

Christison, J.T., D.W. Murray and K.O. Anderson, "Stress Prediction and Low Temperature Fracture Susceptibility of Asphaltic Concrete Pavements," *Journal of the Association of Asphalt Paving Technologist,* Vol. 41, pp. 494-523, 1972.

Ferry, J.D., Viscoelastic properties of polymers, 3rd ed., Wiley, New York, 1980.

Finn, F., C.L. Saraf, R. Kulkarni, K. Nair, W. Smith, and A. Abdullah, "Development of Pavement Subsystems," NCHRP Report 291, Transportation Research Board, Washington DC, 1986.

Flintsch, G.W., I.L. Al-Qadi, A. Loulizi, and D. Mokarem, "Laboratory Tests for Hot-Mix Asphalt Characterization in Virginia," VTRC Report 05-CR22, Charlottesville, VA, 2005.

Fromm, H.J. and W.A. Phang, "A Study of Transverse Cracking of Bituminous Pavements," *Proceedings, Association of Asphalt Paving Technologists,* Vol. 41, pp. 383-423, 1972.

Hafez, I. "Development of a Simplified Asphalt Mix Stability Procedure for Use in Superpave Volumetric Mix Design," Ph.D. Dissertation, Civil Engineering Department, University of Maryland, College Park, MD, 1997.

Hass, R., F. Meyer, G. Assaf, and H. Lee, "A Comprehensive Study of Cold Climate Airport Pavement Cracking," *Proceedings, Association of Asphalt Paving Technologists,* Vol. 56, pp. 198-245, 1987.

Hills, J.F. and D. Brien, "The Fracture of Bitumens and Asphalt Mixes by Temperature Induced Stresses," Prepared Discussion, *Proceedings, Association of Asphalt Paving Technologists,* Vol. 35, pp. 292-309, 1966

Hiltunen, D.R. and R. Roque, “A Mechanics-Based Prediction Model for Thermal Cracking of Asphaltic Concrete Pavements,” *Journal of the Association of Asphalt Paving Technologists,* Vol. 63, pp. 81-117, 1994.

Hiltunen, D.R. and R. Roque, “The Use of Time-Temperature Superposition to Fundamentally Characterize Asphaltic Concrete Mixtures at Low Temperatures,” Engineering Properties of Asphalt Mixtures and the Relationship to their Performance, ASTM STP 1265, Gerald A. Huber and Dale S. Decker, Eds., American Society for Testing and Materials, Philadelphia, 1995.

Huang, Y.H., Pavement Analysis and Design, Englewood Cliffs, N.J.: Prentice-Hall, Inc., 1993.

InstroTek Inc., CoreLok Operators Guide, 2003.

Kim, Y.R., J.S. Daniel and H. Wen, “Fatigue Evaluation of WesTrack Asphalt Mixtures Using Viscoelastic Continuum Damage Approach,” Final Report, North Carolina Department of Transportation, Research Project No. HWY-0678, Raleigh, NC, 2002.

Leaderman, H., “Viscoelasticity phenomena in amorphous high polymeric systems,” *Rheology*, Vol. II, F.R. Eirich, ed., Academic, New York, 1958.

Lakes, R. S., Viscoelastic Solids, Boca Raton, FL: CRC Press LLC, 1999.

Lytton, R.L., U. Shanmugham and B.D. Garrett, “Design of Asphalt Pavements for Thermal Fatigue Cracking,” Research Report 284-4, Texas Transportation Institute, 1983.

McLeod, N.W., “A 4-year Survey of Low-Temperature Transverse Pavement Cracking on Three Ontario Test-Roads,” *Proceedings, Association of Asphalt Paving Technologists,* Vol. 41, 1972.

Molenaar, A.A.A., *Structural Performance and Design of Flexible Road Constructions and Asphalt Concrete Overlays,* Ph.D. Dissertation, Delft University of Technology, Netherlands, 1983.

Painter, P.C. and M.M. Coleman, Fundamentals of Polymer Science – An Introductory Text, Technomic Publishing Co.Inc., ISBN 1-56676-559-5, Lancaster, PA, 1997.

Paris, P.C. and F. Erdogan, “A Critical Analysis of Crack Propagation Laws,” Transactions of the ASME, *Journal of Basic Engineering*, Series D, 85, No. 3, 1963.

Park, S.W. and R.A. Schapery, “Methods of interconversion between linear viscoelastic material functions. Part I-a numerical method based on Prony series,” *International Journal of Solids and Structures,* Vol. 36, pp. 1653-1675, 1999.

Park, S.W. and Y.R. Kim, “Interconversion between Relaxation Modulus and Creep Compliance for Viscoelastic Solids,” *ASCE Journal of Materials in Civil Engineering,* Vol. 11, No. 1, pp. 76-82, 1999.

Park, S.W. and Y.R. Kim, “Fitting Prony-Series Viscoelastic Models with Power-Law Pre-Smoothing,” *ASCE Journal of Materials in Civil Engineering,* Vol. 13, No. 1, pp.26-32, 2001.

Pellinen, T.K. and M.W. Witczak, “Stress Dependent Master Curve Construction for Dynamic (Complex) Modulus,” *Journal of the Association of Asphalt Paving Technologists,* Vol. 71, 2004.

Roque, R., D.H. Hiltunen, W.G. Buttlar, and T. Farwana, “Development of the SHRP Superpave Mixture Specification Test Method to Control Thermal Cracking Performance of Pavements,” Engineering Properties of Asphalt Mixtures and the Relationship to their Performance, ASTM STP 1265, Gerald A. Huber and Dale S. Decker, Eds., American Society for Testing and Materials, Philadelphia, 1995.

Schapery, R.A. and S.W. Park, “Methods of interconversion between linear viscoelastic material functions. Part II-an approximate analytical method,” *International Journal of Solids and Structures,* Vol. 36, pp. 1677-1699, 1999.

Witczak, M.W., R. Roque, D.R. Hiltunen, and W.G. Buttlar, “Modification and Re-Calibration of Superpave Thermal Cracking Model,” NCHRP 9-19 Project Report, Arizona State University Department of Civil and Environmental Engineering, Tempe, Arizona, December 2000.

Witczak, M.W., K. Kaloush, T.K. Pellinen, M. El-Basyouny, and H. Von Quitus, “Simple Performance Test for Superpave Mix Design,” NCHRP Report 465, Transportation Research Board, Washington DC, 2002.

Appendix A: Fitting model SAS Input and Output

A.1 Prony series model

1. Uniaxial BM

```
data uniaxialBM;
input time gr;
lines;
.
.
(data here)
.
.
proc nlin;
model   gr=ga0   +ga1*(1-exp(-time/tau1))+ga2*(1-exp(-time/tau2))+ga3*(1-exp(-
time/tau3))+ga4*(1-exp(-time/tau4))+ga5*(1-exp(-time/tau5));
parms ga0=0.05 ga1=1.0 ga2=3.0 ga3=8.0 ga4=7.0 ga5=7.0 tau1=1 tau2=8 tau3=98
tau4=980 tau5=9800;
bounds ga0 > 0;
bounds ga1 > 0;
bounds ga2 > 0;
bounds ga3 > 0;
bounds ga4 > 0;
bounds ga5 > 0;
run;
```

Estimation Summary

Method	Gauss-Newton
Iterations	17
R	7.692E-6
PPC(tau1)	0.000062
RPC(tau1)	0.000102
Object	2.56E-10
Objective	74.27335
Observations Read	4990
Observations Used	4990
Observations Missing	0

Source	DF	Sum of Squares	Mean Square	Approx F Value	Pr > F
Regression	11	330054	30004.9	1052231	<.0001
Residual	4979	74.2734	0.0149		
Uncorrected Total	4990	330129			
Corrected Total	4989	157039			

Parameter	Estimate	Approx Std Error	Approximate 95% Confidence Limits	
ga0	0.0695	0.00384	0.0620	0.0771
ga1	0.3534	0.0264	0.3017	0.4052
tau1	1.0739	0.1274	0.8241	1.3237

ga2	1.3200	0.0361	1.2493	1.3907
tau2	17.6127	1.4402	14.7893	20.4361
ga3	2.8247	0.0362	2.7537	2.8958
tau3	184.1	3.9147	176.4	191.7
ga4	6.9871	0.0322	6.9239	7.0502
tau4	3100.9	28.2353	3045.6	3156.3
ga5	8.2219	0.1243	7.9782	8.4656
tau5	52695.4	1854.6	49059.4	56331.3

2. Uniaxial SM

```
data uniaxialSM;
input time gr;
lines;
.
.
(data here)
.
.
proc nlin;
model   gr=ga0   +ga1*(1-exp(-time/tau1))+ga2*(1-exp(-time/tau2))+ga3*(1-exp(-
time/tau3))+ga4*(1-exp(-time/tau4))+ga5*(1-exp(-time/tau5));
parms ga0=0.1 ga1=2.0 ga2=0.1 ga3=6.0 ga4=3.0 ga5=3.0 tau1=1 tau2=8 tau3=98
tau4=980 tau5=9800;
bounds ga0 > 0;
bounds ga1 > 0;
bounds ga2 > 0;
bounds ga3 > 0;
bounds ga4 > 0;
bounds ga5 > 0;
run;
```

Estimation Summary

Subiterations	9
Average Subiterations	0.257143
R	6.287E-6
PPC(tau1)	9.436E-6
RPC(tau1)	0.000019
Object	2.36E-10
Objective	15.81518
Observations Read	4982
Observations Used	4982
Observations Missing	0

Source	DF	Sum of Squares	Mean Square	Approx F Value	Pr > F
Regression	11	231710	21064.5	3223141	<.0001
Residual	4971	15.8152	0.00318		

Uncorrected Total	4982	231725
Corrected Total	4981	102560

Parameter	Estimate	Approx Std Error	Approximate 95% Confidence Limits	
ga0	0.1779	0.00181	0.1743	0.1814
ga1	0.5667	0.00399	0.5589	0.5745
tau1	1.1788	0.0283	1.1234	1.2342
ga2	2.2899	0.0106	2.2692	2.3106
tau2	62.7561	0.7181	61.3483	64.1639
ga3	3.3976	0.0131	3.3719	3.4233
tau3	779.3	6.0910	767.4	791.3
ga4	3.3472	0.0812	3.1881	3.5064
tau4	9977.3	229.5	9527.4	10427.2
ga5	4.7423	0.0409	4.6622	4.8225
tau5	55521.0	2151.8	51302.4	59739.6

3. IDT BM

```
data IDTBM;
input time gr;
lines;
.
.
(data here)
.
.
proc nlin;
model   gr=ga0   +ga1*(1-exp(-time/tau1))+ga2*(1-exp(-time/tau2))+ga3*(1-exp(-
time/tau3))+ga4*(1-exp(-time/tau4))+ga5*(1-exp(-time/tau5));
parms ga0=0.3 ga1=29 ga2=3.8 ga3=31 ga4=50.0 ga5=50.0 tau1=1 tau2=8 tau3=98
tau4=980 tau5=9800;
bounds ga0 > 0;
bounds ga1 > 0;
bounds ga2 > 0;
bounds ga3 > 0;
bounds ga4 > 0;
bounds ga5 > 0;
run;
```

Estimation Summary	
Subiterations	10
Average Subiterations	0.37037
R	9.59E-6
PPC(tau1)	0.000296
RPC(tau1)	0.000429
Object	6E-11
Objective	1507.267
Observations Read	4743
Observations Used	4743

Observations Missing 0

Source	DF	Sum of Squares	Mean Square	Approx F Value	Pr > F
Regression	11	10819582	983598	2007677	<.0001
Residual	4732	1507.3	0.3185		
Uncorrected Total	4743	10821089			
Corrected Total	4742	6396490			

Parameter	Estimate	Approx Std Error	Approximate 95% Confidence Limits	
ga0	0.0719	0.0546	-0.0353	0.1790
ga1	0.2184	0.0670	0.0870	0.3499
tau1	1.1480	1.5437	-1.8784	4.1745
ga2	2.0212	0.0615	1.9007	2.1418
tau2	69.7343	4.9473	60.0351	79.4335
ga3	44.5864	0.3249	43.9494	45.2234
tau3	28522.1	381.8	27773.5	29270.7
ga4	13.6771	0.1998	13.2854	14.0688
tau4	3235.2	85.0522	3068.4	3401.9
ga5	50.4167	0.1980	50.0285	50.8050
tau5	202826	4176.7	194637	211014

4. IDT SM

```
data IDT SM;
input time gr;
lines;
.
.
(data here)
.
.
proc nlin;
model   gr=ga0   +ga1*(1-exp(-time/tau1))+ga2*(1-exp(-time/tau2))+ga3*(1-exp(-
time/tau3))+ga4*(1-exp(-time/tau4))+ga5*(1-exp(-time/tau5));
parms  ga0=0.1  ga1=2.0  ga2=10.0  ga3=40.0  ga4=50.0  ga5=50.0  tau1=1  tau2=8
tau3=98 tau4=980 tau5=9800;
bounds ga0 > 0;
bounds ga1 > 0;
bounds ga2 > 0;
bounds ga3 > 0;
bounds ga4 > 0;
bounds ga5 > 0;
run;
```

Estimation Summary

Subiterations	86
Average Subiterations	1.457627
R	9.018E-6
PPC(tau1)	0.000046
RPC(tau1)	0.000071
Object	6.89E-11
Objective	25.40781
Observations Read	4749
Observations Used	4749
Observations Missing	0

Source	DF	Sum of Squares	Mean Square	Approx F Value	Pr > F
Regression	11	134991	12271.9	1347524	<.0001
Residual	4738	25.4078	0.00536		
Uncorrected Total	4749	135017			
Corrected Total	4748	72287.2			

Parameter	Estimate	Approx Std Error	Approximate 95% Confidence Limits	
ga0	0.0846	0.00326	0.0782	0.0910
ga1	0.2835	0.00978	0.2644	0.3027
tau1	9.1336	0.9879	7.1969	11.0703
ga2	1.0769	0.0169	1.0438	1.1100
tau2	167.1	4.6577	157.9	176.2
ga3	6.0480	0.0652	5.9201	6.1759
tau3	16307.7	272.0	15774.5	16840.9
ga4	2.0710	0.0190	2.0338	2.1083
tau4	1501.4	36.0143	1430.8	1572.0
ga5	4.0234	0.1067	3.8142	4.2326
tau5	159088	14878.1	129919	188257

A.2 Power model

1. Uniaxial BM

```
data Uniaxial BM;
input time gr;
lines;
.
.
(data here)
.
.
proc nlin;
model gr=ga0+ga1*time**mval;
parms ga0=0.065 ga1=0.25 mval=0.5;
bounds ga0 > 0;
bounds ga1 > 0;
run;
```

Estimation Summary

Method	Gauss-Newton
Iterations	5
R	3.655E-6
PPC(ga0)	6.212E-6
RPC(ga0)	0.000161
Object	8.578E-9
Objective	2.927462
Observations Read	2183
Observations Used	2183
Observations Missing	0

Source	DF	Sum of Squares	Mean Square	Approx F Value	Pr > F
Regression	3	2230.9	743.6	561593	<.0001
Residual	2180	2.9275	0.00134		
Uncorrected Total	2183	2233.8			
Corrected Total	2182	1511.2			

Parameter	Estimate	Approx Std Error	Approximate 95% Confidence Limits	
ga0	0.0246	0.00130	0.0220	0.0271
ga1	0.3951	0.00142	0.3923	0.3979
mval	0.4497	0.000738	0.4483	0.4511

2. Uniaxial SM

```
data Uniaxial SM;
input time gr;
lines;
.
.
(data here)
.
.
proc nlin;
model gr=ga0 +ga1*time**mval;
parms ga0=0.065 ga1=0.5 mval=0.3;
bounds ga0 > 0;
bounds ga1 > 0;
run;
```

Estimation Summary

Method	Gauss-Newton
Iterations	5
R	4.162E-6
PPC(ga0)	6.817E-6
RPC(ga0)	0.000114
Object	4.539E-9
Objective	12.28292
Observations Read	2614
Observations Used	2614
Observations Missing	0

Source	DF	Sum of Squares	Mean Square	Approx F Value	Pr > F
Regression	3	10909.3	3636.4	672038	<.0001
Residual	2611	12.2829	0.00470		
Uncorrected Total	2614	10921.6			
Corrected Total	2613	6335.2			

Parameter	Estimate	Approx Std Error	Approximate 95% Confidence Limits	
ga0	0.0656	0.00272	0.0603	0.0709
ga1	0.5024	0.00271	0.4971	0.5078
mval	0.3681	0.000853	0.3664	0.3697

3. IDT BM

```
data IDT BM;
input time gr;
lines;
.
.
(data here)
.
.
proc nlin;
model gr=ga0 +ga1*time**mval;
parms ga0=0.00001 ga1=0.3 mval=0.4;
bounds ga0 > 0;
bounds ga1 > 0;
run;
```

Estimation Summary

Method	Gauss-Newton
Iterations	39
Subiterations	231
Average Subiterations	5.923077
R	2.25E-6
PPC(ga1)	1.542E-6
RPC(ga1)	0.000014
Object	3.78E-10
Objective	6532.418
Observations Read	3730
Observations Used	3730
Observations Missing	0

Source	DF	Sum of Squares	Mean Square	Approx F Value	Pr > F
Regression	2	2789760	1394880	1123080	<.0001
Residual	3728	6532.4	1.7523		
Uncorrected Total	3730	2796293			
Corrected Total	3729	1974458			

Parameter	Estimate	Approx Std Error	Approximate 95% Confidence Limits		Label
ga0	1E-8	0	1E-8	1E-8	
ga1	0.3022	0.00340	0.2955	0.3088	
mval	0.4953	0.00106	0.4932	0.4974	

Bound1	1081.1	49.8802	983.3	1178.8	0 < ga0

4. IDT SM

```
data IDT SM;
input time gr;
lines;
.
.
(data here)
.
.
proc nlin;
model gr=ga0 +ga1*time**mval;
parms ga0=0.00001 ga1=0.2 mval=0.3;
bounds ga0 > 0;
bounds ga1 > 0;
run;
```

Estimation Summary

Method	Gauss-Newton
Iterations	9
Subiterations	16
Average Subiterations	1.777778
R	4.581E-7
PPC(ga1)	1.231E-7
RPC(ga1)	3.121E-6
Object	1.3E-10
Objective	35.11679
Observations Read	3809
Observations Used	3809
Observations Missing	0

Source	DF	Sum of Squares	Mean Square	Approx F Value	Pr > F
Regression	2	22446.1	11223.0	1021009	<.0001
Residual	3807	35.1168	0.00922		
Uncorrected Total	3809	22481.2			
Corrected Total	3808	9453.2			

Parameter	Estimate	Approx Std Error	Approximate 95% Confidence Limits		Label
ga0	1E-8	0	1E-8	1E-8	
ga1	0.1760	0.000775	0.1745	0.1775	
mval	0.3990	0.000576	0.3979	0.4002	
Bound1	53.4334	2.2710	48.9826	57.8842	0 < ga0

A.3 Sigmoidal model

1. Uniaxial BM

```
data Uniaxial BM;
input time gr;
lines;
.
.
(data here)
.
.
proc nlin;
model gr=ga0+ga1/(1+exp(ga2+ga3*time));
parms ga0=0.1 ga1=1 ga2=1 ga3=1;
run;
```

Estimation Summary

Method	Gauss-Newton
Iterations	10
Subiterations	2
Average Subiterations	0.2
R	2.736E-6
PPC(ga2)	1.123E-6
RPC(ga2)	9.506E-6
Object	4.73E-10
Objective	5.368084
Observations Read	4982
Observations Used	4982
Observations Missing	0

Source	DF	Sum of Squares	Mean Square	Approx F Value	Pr > F
Regression	4	4174.1	1043.5	1170581	<.0001
Residual	4978	5.3681	0.00108		
Uncorrected Total	4982	4179.5			
Corrected Total	4981	3792.3			

Parameter	Estimate	Std Error	Approx Approximate 95% Confidence Limits	
ga0	1.4138	0.00329	1.4074	1.4203
ga1	-2.8726	0.00618	-2.8847	-2.8605
ga2	-0.5693	0.00350	-0.5762	-0.5624
ga3	0.6602	0.00248	0.6553	0.6650

2. Uniaxial SM

```
data Uniaxial SM;
input time gr;
lines;
.
.
(data here)
.
.
proc nlin;
model gr=ga0+ga1/(1+exp(ga2+ga3*time));
parms ga0=0.1 ga1=1 ga2=1 ga3=1;
run;
```

Estimation Summary

Method	Gauss-Newton
Iterations	9
Subiterations	2
Average Subiterations	0.222222
R	1.348E-6
PPC(ga2)	3.569E-7
RPC(ga2)	8.882E-6
Object	1.072E-9
Objective	1.77062
Observations Read	4982
Observations Used	4982
Observations Missing	0

Source	DF	Sum of Squares	Mean Square	Approx F Value	Pr > F
Regression	4	2954.7	738.7	2181328	<.0001
Residual	4978	1.7706	0.000356		
Uncorrected Total	4982	2956.4			
Corrected Total	4981	2329.4			

Parameter	Estimate	Std Error	Approx Approximate 95% Confidence Limits	
ga0	1.2825	0.00184	1.2788	1.2861
ga1	-2.2737	0.00350	-2.2805	-2.2668
ga2	-0.7796	0.00294	-0.7854	-0.7739
ga3	0.6694	0.00176	0.6659	0.6728

3. IDT BM

```
data IDT BM;
input time gr;
lines;
.
.
(data here)
.
.
proc nlin;
model gr=ga0+ga1/(1+exp(ga2+ga3*time));
parms ga0=0.1 ga1=1 ga2=1 ga3=1;
run;
```

Estimation Summary

Method	Gauss-Newton
Iterations	12
Subiterations	9
Average Subiterations	0.75
R	5.193E-6
PPC(ga3)	1.8E-6
RPC(ga3)	0.000018
Object	2.537E-9
Objective	5.546655
Observations Read	4743
Observations Used	4743
Observations Missing	0

Source	DF	Sum of Squares	Mean Square	Approx F Value	Pr > F
Regression	4	7801.9	1950.5	1497821	<.0001
Residual	4739	5.5467	0.00117		
Uncorrected Total	4743	7807.4			
Corrected Total	4742	5264.8			

Parameter	Estimate	Approx Std Error	Approximate 95% Confidence Limits	
ga0	2.7379	0.00928	2.7197	2.7561
ga1	-4.4302	0.0175	-4.4646	-4.3958
ga2	-1.2069	0.00673	-1.2201	-1.1937
ga3	0.5275	0.00287	0.5219	0.5331

4. IDT SM

```
data IDT SM;
input time gr;
lines;
.
.
(data here)
.
.
proc nlin;
model gr=ga0+ga1/(1+exp(ga2+ga3*time));
parms ga0=0.1 ga1=1 ga2=1 ga3=1;
run;
```

Estimation Summary

Method	Gauss-Newton
Iterations	8
Subiterations	6
Average Subiterations	0.75
R	6.396E-7
PPC(ga2)	1.387E-7
RPC(ga2)	0.000019
Object	6.187E-9
Objective	1.320332
Observations Read	4749
Observations Used	4749
Observations Missing	0

Source	DF	Sum of Squares	Mean Square	Approx F Value	Pr > F
Regression	4	2295.9	574.0	2510806	<.0001
Residual	4745	1.3203	0.000278		
Uncorrected Total	4749	2297.2			
Corrected Total	4748	2097.3			

Parameter	Estimate	Std Error	Approx Approximate 95% Confidence Limits	
ga0	1.4459	0.00336	1.4394	1.4525
ga1	-3.2149	0.0100	-3.2345	-3.1952
ga2	-0.9598	0.00670	-0.9730	-0.9467
ga3	0.5907	0.00234	0.5861	0.5953

VITA

Myunggoo Jeong was born in Seoul, Korea, on October 15, 1972. He attended Sung Kyun Kwan University with honor in 1991. One year after the completion of his undergraduate study, he served in the Korean Air Force as part of required 30-month military service. After finishing the military service, he resumed his undergraduate study and graduated with a Bachelor of Science degree in Civil Engineering in 1998.

Upon graduation, he joined the Samsung Engineering Construction Company (SECC) as a civil engineer. He worked at two construction sites where he built new and remodeled existing highways. After four year of work, he decided to return to school and enrolled at Virginia Polytechnic Institute and State University, Blacksburg, Virginia in August, 2003. He has served as a graduate research assistant since 2004 under the direction of Dr. Flintsch and earned a Master of Science Degree in Civil and Environmental Engineering in 2005. He intends to pursue a Ph. D degree at Arizona State University from August 2005.